Sommer M, Bertsch D, Dingus B, Fichtel C, Fishman G, et al. 1994. *Ap. J. Lett.* 422:L63–66
Strohmeyer TE, Fenimore EE, Miralles JA. 1994. *Ap. J.* 432:665–71
Terekhov OV, Denisenko DV, Lobachev VA, Sunyaev RA, Kovtun AV. 1994. *Astron. Lett.* 20:265–99
Ulmer A, Wijers R. 1995. *Ap. J.* 439:303–306
Ulmer A, Wijers R., Fenimore E. 1995. *Ap. J. Lett.* 440:L9–12
Usov V. 1992. *Nature* 357:472–74
Usov V, Chibisov G. 1975. *Sov. Astron.* 19:115–16
van den Berg S. 1983. *Astrophys. Space Sci.* 97:385–88
Vanderspek R, Krimm H, Ricker G. 1994. In HUNTSVILLE 2, pp. 438–43
Vedrenne G. 1991. *Ann. NY Acad. Sci.* 647:556–74
Vrba F, Hartmann D, Jennings M. 1994. In HUNTSVILLE 2, pp. 443–47
Wambsganss J. 1993. *Ap. J.* 406:29–35
Wang V, Lingenfelter R. 1993. *Ap. J. Lett.* 416:L13–16
Wasserman I. 1992. *Ap. J.* 394:565–73
White S. 1993. *Astrophys. Space Sci.* 208:301–11
White S. 1994. In HUNTSVILLE 2, pp. 620–24
Wickramasinghe W, Nemiroff R, Norris J, Kouveliotou C, Fishman G, et al. 1993. *Ap. J. Lett.* 411:L55–58
Wilson R, Fishman G, Meegan C. 1982. In *Gamma-Ray Transients and Related Astrophysical Phenomena*, ed. RE Lingenfelter, HS Hudson, DM Worrall, *AIP Conf. Proc.* 77:67–70. New York: Am. Inst. Phys.
Winkler C, Bennett K, Bloemen H, Collmar W, Connors A, et al. 1992. *Astron. Astrophys.* 255:L9–12
Wijers R, Paczyński B. 1994. *Ap. J. Lett.* 437:L107–10
Woods E, Loeb A. 1994. *Ap. J.* 425:L63–66
Woosley S. 1993. *Ap. J.* 405:273–77
Yi I. 1994. *Ap. J.* 431:543–58
Yoshida A, Murakami T, Itoh M, Nishimura J, Tsuchiya T. et al. 1989. *Publ. Astron. Soc. Jpn.* 41:509–18
Yoshida A, Murakami T, Nishimura J, Kondo I, Fenimore E. 1992. In TAOS, pp. 399–406
Zytkow A. 1990. *Ap. J.* 359:138–54

Annu. Rev. Astron. Astrophys. 1995. 33:459–503

OPTIONAL EXTRA READING ON:

THE SOLAR NEUTRINO PROBLEM[1]

W. C. Haxton

Institute for Nuclear Theory, NK-12, and Department of Physics, FM-15, University of Washington, Seattle, Washington 98195

KEY WORDS: solar models, neutrino oscillations, neutrino detection

ABSTRACT

The solar neutrino problem has persisted for almost three decades. Recent results from Kamiokande, SAGE, and GALLEX indicate a pattern of neutrino fluxes that is very difficult to reconcile with plausible variations in standard solar models. This situation is reviewed, and suggested particle physics solutions are discussed. A summary is given of the important physics expected from SNO, SuperKamiokande, and other future experiments.

1. INTRODUCTION

Thirty years ago, in the summer of 1965, the Homestake Mining Company completed the excavation of the 30 × 60 × 32 ft cavity that was to house the 100,000-gallon chlorine detector proposed by Ray Davis Jr. and his Brookhaven National Laboratory collaborators. Three years later Davis, Harmer & Hoffman (1968) announced the result of their first two detector runs: an upper bound on the solar neutrino flux of 3 SNU [1 SNU $\equiv 10^{-36}$ captures/(target atom)/sec]. In an accompanying theoretical paper, Bahcall, Bahcall & Shaviv (1968) found a rate of 7.5 ± 3.3 SNU for the standard solar model. This discrepancy persists today, augmented by nearly three decades of data from the Homestake experiment and by the new results from the Kamiokande and GALLEX/SAGE detectors. The purpose of this review is to summarize the current status of the solar neutrino problem and its possible implications for physics and astrophysics.

A remarkable aspect of the solar neutrino problem is that it has both endured and deepened. The prospect of quantitatively testing the theory of main-

[1]The US Government has the right to retain a nonexclusive, royalty-free license in and to any copyright covering this paper.

sequence stellar evolution provided much of the original motivation for measuring solar neutrinos: Solar neutrinos carry, in their energy distribution and flux, a precise record of the thermonuclear reactions occurring in the sun's core. Our understanding of the atomic and nuclear microphysics governing stellar evolution—nuclear reaction rates, radiative opacities, and the equation of state—has progressed significantly since the 1960s. The development of helioseismology has provided a new tool for probing the solar interior. Finally, we better understand our sun in the context of other stars, the observations of which have helped to define the envelope of possibilities for diffusion, mass loss, magnetic fields, etc. This progress has tended to increase our confidence in the standard solar model. At the same time, with the new results from Kamiokande and the gallium detectors, a pattern of neutrino fluxes has emerged that is more difficult to reconcile with possible variations in that model.

The solar neutrino problem has deepened because of the discovery of the Mikheyev-Smirnov-Wolfenstein (MSW) mechanism: The sun has the potential to greatly enhance the effects of neutrino mixing. If neutrino oscillations prove to be the solution to the solar neutrino problem, this will force modifications in the standard model of electroweak interactions, which accommodates neither massive neutrinos nor their mixing. This new physics would have implications for a variety of problems in astrophysics, including the missing mass puzzle and the formation of large-scale structure.

There are several sources that the interested reader can consult for additional information. The most comprehensive treatment is that given by Bahcall in his book *Neutrino Astrophysics* (1989). The appendix of this book reprints a delightful historical perspective of the development of the solar neutrino problem (Bahcall & Davis 1982). The review by Bowles & Gavrin (1993) provides an excellent discussion of the Homestake, Kamiokande, and SAGE/GALLEX experiments, as well as detectors now under construction or development. The proceedings of the Seattle Solar Modeling Workshop (Balantekin & Bahcall 1995) and the Homestake Conference (Cherry, Lande & Fowler 1985) contain many studies of the standard and nonstandard solar models and of the nuclear and atomic physics on which such models depend. The theory of matter-enhanced neutrino oscillations has been reviewed recently by Mikheyev & Smirnov (1989).

2. SOLAR MODELS

2.1 *The Standard Solar Model*

Solar models trace the evolution of the sun over the past 4.6 billion years of main sequence burning, thereby predicting the present-day temperature and composition profiles of the solar core that govern neutrino production. Standard solar models share four basic assumptions:

- The sun evolves in hydrostatic equilibrium, maintaining a local balance between the gravitational force and the pressure gradient. To describe this condition in detail, one must specify the equation of state as a function of temperature, density, and composition.

- Energy is transported by radiation and convection. While the solar envelope is convective, radiative transport dominates in the core region where thermonuclear reactions take place. The opacity depends sensitively on the solar composition, particularly the abundances of heavier elements.

- Thermonuclear reaction chains generate solar energy. The standard model predicts that over 98% of this energy is produced from the pp chain conversion of four protons into ^{4}He (see Figure 1),

$$4p \rightarrow {}^4\mathrm{He} + 2e^+ + 2\nu_e, \tag{1}$$

with the CNO cycle contributing the remaining 2%. The sun is a large but slow reactor: The core temperature, $T_c \sim 1.5 \cdot 10^7$ K, results in typical center-of-mass energies for reacting particles of ~10 keV, much less than the Coulomb barriers inhibiting charged particle nuclear reactions. Thus, reaction cross sections are small, and one must go to significantly higher energies before laboratory measurements are feasible. These laboratory data must then be extrapolated to the solar energies of interest.

- The model is constrained to produce today's solar radius, mass, and luminosity. An important assumption of the standard model is that the sun was highly convective, and therefore uniform in composition, when it first

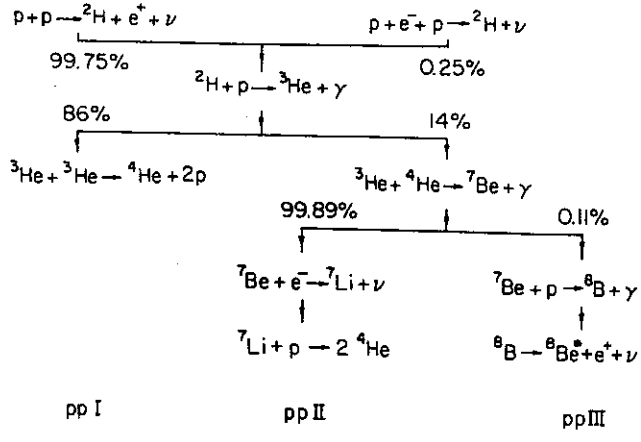

Figure 1 The solar pp chain.

Table 1 Neutrino fluxes predicted by the Bahcall/Pinsonneault (with and without He diffusion) and Turck-Chièze/Lopez standard solar models

Source	E_ν^{max} (MeV)	Flux (cm^{-2} s^{-1}) BP (with diffusion)	BP (without)	TCL
$p + p \rightarrow {}^2H + e^+ + \nu$	0.42	6.00E10	6.04E10	6.03E10
${}^{13}N \rightarrow {}^{13}C + e^+ + \nu$	1.20	4.92E8	4.35E8	3.83E8
${}^{15}O \rightarrow {}^{15}N + e^+ + \nu$	1.73	4.26E8	3.72E8	3.18E8
${}^{17}F \rightarrow {}^{17}O + e^+ + \nu$	1.74	5.39E6	4.67E6	
${}^8B \rightarrow {}^8Be + e^+ + \nu$	~15	5.69E6	5.06E6	4.43E6
${}^3He + p \rightarrow {}^4He + e^+ + \nu$	18.77	1.23E3	1.25E3	
${}^7Be + e^- \rightarrow {}^7Li + \nu$	0.86(90%)	4.89E9	4.61E9	4.34E9
	0.38(10%)			
$p + e^- + p \rightarrow {}^2H + \nu$	1.44	1.43E8	1.43E8	1.39E8

entered the main sequence. It is furthermore assumed that the surface abundances of metals (nuclei with A >5) were undisturbed by the subsequent evolution, and thus provide a record of the initial solar metallicity. The remaining parameter is the initial ^{4}He/H ratio, which is adjusted until the model reproduces the present solar luminosity after 4.6 billion years of evolution. The resulting ^{4}He/H mass fraction ratio is typically 0.27 ± 0.01, which can be compared to the big bang value of 0.23 ± 0.01 (Walker et al 1991). Note that the sun was formed from previously processed material.

The model that emerges is one of an evolving sun. As the core's chemical composition changes, the opacity and core temperature rise, producing a 44% luminosity increase since the onset of the main sequence. The ^{8}B neutrino flux, the most temperature-dependent component, proves to be of relatively recent origin: The predicted flux increases exponentially with a doubling period of about 0.9 billion years. The equilibrium abundance and equilibration time for ^{3}He are both sharply increasing functions of the distance from the solar center. Thus a steep ^{3}He density gradient is established over time.

The principal neutrino-producing reactions of the pp chain and CNO cycle are summarized in Table 1. The first six reactions produce β decay neutrino spectra having allowed shapes with endpoints given by E_ν^{max}. Deviations from an allowed spectrum occur for ^{8}B neutrinos because the ^{8}Be final state is a broad resonance (Bahcall & Holstein 1986); much smaller deviations occur because of second-forbidden contributions to the decay. The last two reactions produce line sources of electron capture neutrinos, with widths ~2 keV that are characteristic of the solar core temperature (Bahcall 1993). The resulting solar neutrino spectrum is shown in Figure 2.

Measurements of the pp, ^{7}Be, and ^{8}B neutrino fluxes will determine the relative contributions of the ppI, ppII, and ppIII cycles to solar energy generation. As the discusion below illustrates, this competition is governed in large classes of solar models by a single parameter, the central temperature T_c. The flux predictions of two standard models, those of Bahcall & Pinsonneault (1992) and of Turck-Chièze and Lopez (1993), are included in Table 1.

2.2 *Uncertainties in Standard Solar Model Parameters*

Careful analyses of the experiments to be described in Section 3 indicate that the observed solar neutrino fluxes differ substantially from standard solar model (SSM) expectations (White, Krauss & Gates 1993; Parke 1995; Hata & Langacker 1994). These analyses find

$$\begin{aligned} \phi(\mathrm{pp}) &\sim 0.9\,\phi^{\mathrm{SSM}}(\mathrm{pp}) \\ \phi(^7\mathrm{Be}) &\sim 0 \\ \phi(^8\mathrm{B}) &\sim 0.43\,\phi^{\mathrm{SSM}}(^8\mathrm{B}). \end{aligned} \tag{2}$$

Reduced ^{7}Be and ^{8}B neutrino fluxes can be produced by lowering the central temperature of the sun somewhat. However, such adjustments, either by varying

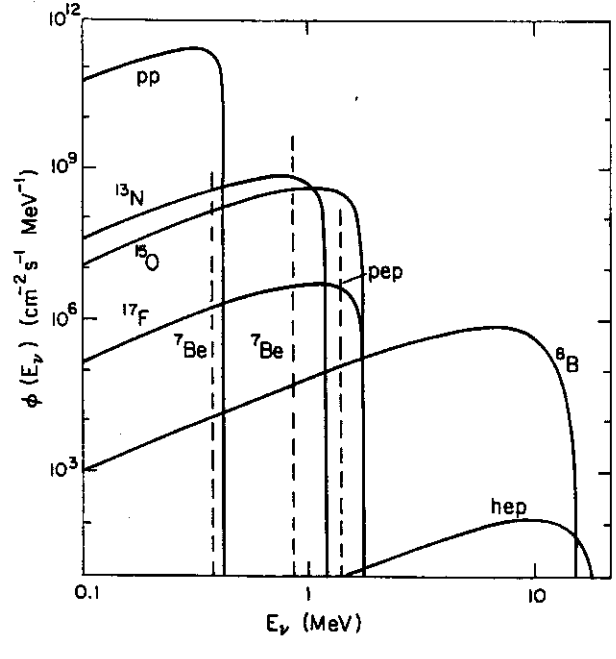

Figure 2 The flux densities (*solid lines*) of the principal β decay sources of solar neutrinos of the standard solar model. The total fluxes are those of the BP SSM. The ^{7}Be and pep electron capture neutrino fluxes (*dashed lines*) are discrete and given in units of cm^{-2} s^{-1}.

the parameters of the SSM or by adopting some nonstandard physics, tend to push the $\phi(^7\mathrm{Be})/\phi(^8\mathrm{B})$ ratio to higher values rather than the low one of Equation (2),

$$\frac{\phi(^7\mathrm{Be})}{\phi(^8\mathrm{B})} \sim T_c^{-10}. \tag{3}$$

Thus, the observations seem difficult to reconcile with plausible solar model variations.

It is apparent that the rigor of this argument is the crucial issue: How quantitative is the tracking of fluxes and flux ratios with T_c, what variations can exist in models that produce the same T_c but differ in other respects, and how significant are the results in Equation (2) when the statistical and systematic errors of the experiments are taken into account? These questions have motivated a number of careful examinations (and clever presentations) of solar model uncertainties.

SSM uncertainties include the reaction cross sections for the pp chain and CNO cycle, the opacities, the deduction of heavy element abundances from solar surface abundances, the solar age and present day luminosity, and the equation of state. Modelers occasionally adopt different "best values" and associated errors for these parameters. Bahcall & Pinsonneault (1992) have argued that the differences among solar models are almost always attributable to parameter choices and not to disagreements about the underlying physics.

While a detailed summary of standard model uncertainties would take us well beyond the limits of this review, a qualitative discussion of pp chain uncertainties is appropriate. This nuclear microphysics has been the focus of a great deal of experimental work, as well as the source of some contention among modelers. The pp chain involves a series of nonresonant charged-particle reactions occurring at center-of-mass energies that are well below the height of the inhibiting Coulomb barriers. Because the resulting small cross sections preclude laboratory measurements at the relevant energies, one must extrapolate higher energy measurements to threshold to obtain solar cross sections. This extrapolation is often discussed in terms of the astrophysical S-factor (Fowler 1984, Burbidge et al 1957),

$$\sigma(E) = \frac{S(E)}{E}\exp(-2\pi\eta) \tag{4}$$

where $\eta = (Z_1 Z_2 \alpha)/\beta$; α is the fine structure constant, and $\beta = v/c$ the relative velocity of the colliding particles. This parameterization removes the gross Coulomb effects associated with the s-wave interactions of charged, point-like particles. The remaining energy dependence of $S(E)$ is gentle and can be expressed as a low-order polynomial in E. Usually the variation of $S(E)$ with E is taken from a direct reaction model and then used to extrapolate

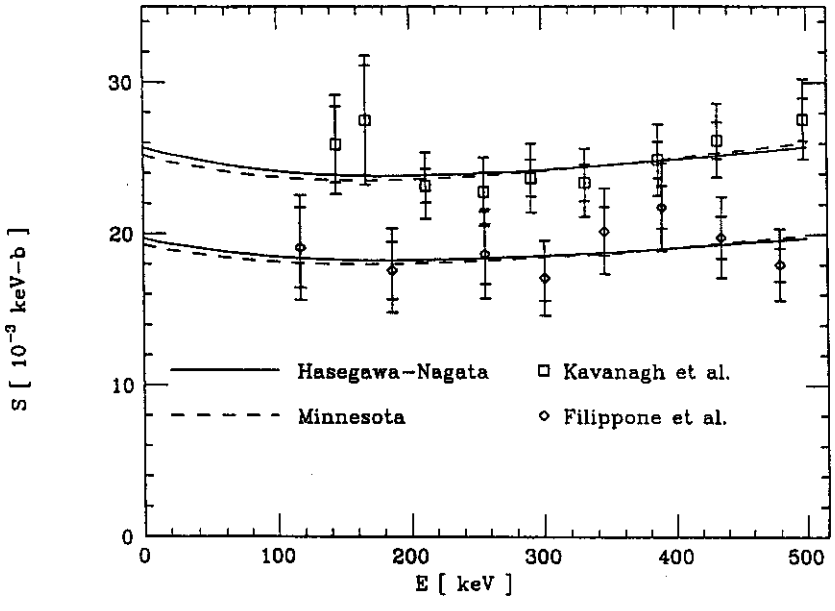

Figure 3 The ^{7}Be(p, γ)^{8}B S-factors as measured by Kavanagh et al (1969) and by Filippone et al (1983). For each data set, two theoretical extrapolations, reflecting different choices for the strong potentials, to $S(0)$ are shown (Johnson et al 1992). The enlargement of the error bars is a correction by these authors to account for the systematic differences in the two data sets.

higher energy measurements to threshold. The model accounts for finite nuclear size effects, strong interaction effects, contributions from other partial waves, etc. Because laboratory measurements are made with atomic nuclei, whereas conditions in the solar core guarantee the complete ionization of light nuclei, additional corrections must be made to account for the different electronic screening environments.

Among the pp chain reactions, the one presently most controversial is ^{7}Be(p, γ)^{8}B. The two experiments performed at the lowest energies (Kavanagh et al 1969, Filippone et al 1983) find very similar energy dependences but disagree in overall normalization by about 25%. A similar normalization disagreement exists among higher energy data sets (see Langanke 1995, Parker 1968, Kavanagh et al 1969, Vaughn et al 1970).

Theory predicts a threshold energy dependence for $S(E)$ that rises gently as $E \to 0$; at sufficiently low energies, when the capture occurs at nuclear separations well outside the range of nuclear forces, the behavior is fixed (Christy & Duck 1961, Williams & Koonin 1981). The data are consistent with theory, though their accuracy at low energies (120–200 keV) is insufficient to independently determine the rise at low E (see Figure 3). When the theoretical

energy dependence (Johnson et al 1992) of $S(E)$ is used to extrapolate the Kavanagh et al and Filippone et al data, one finds $S(0) \sim 25$ and ~ 20 eV barns, respectively. While most calculations have predicted values for $S(0)$ closer to the Kavanagh value, lower values have also been obtained (see, e.g. Xu et al 1994) and general arguments have been given that the theoretical normalization uncertainty could be as much as a factor of two (Barker 1980). Thus it does not appear that theory can distinguish between competing experimental normalizations for $S(0)$. In the most recent reexamination of the data, Johnson et al (1992) determined $S_{17}(0) = 22.4 \pm 2.1$ eV barns, from a weighted average of six data sets.

Very recently Motobayashi et al (1994), by measuring the breakup of ^{8}B in the Coulomb field of ^{208}Pb, deduced a preliminary value of $S_{17}(0) = 16.7 \pm 3.2$ eV barns, which would favor the Filippone result. It has been argued that the extraction of $S_{17}(0)$ from the Coulomb breakup cross section is complicated by the three-body Coulomb effects in the outgoing channel and by larger E2 contributions (Langanke & Shoppa 1994), though this claim has been disputed (Gai & Bertulani 1994). (Transverse electric multipoles of the electromagnetic current operator of rank J are denoted EJ.)

The SSM calculations of Bahcall & Ulrich (1988) and Turck-Chièze et al (1988) adopted $S_{17}(0)$ values of 24.3 ± 1.8 eV b and 21 ± 3 eV b, respectively. This was the most important contribution to the differences in their flux predictions. Their recently updated calculations (Bahcall & Pinsonneault 1992, Turck-Chièze & Lopez 1993) both adopt the Johnson et al central value, though Turck-Chièze and Lopez assign a larger error bar to this result because of the concern that the weighted average of Johnson et al does not fully reflect the systematic disagreement illustrated in Figure 3.

While there has been some movement to lower values of $S_{17}(0)$, neither the best value nor appropriate error is likely to be decided without additional measurements. The resulting reduction in $\phi(^8\text{B})$, because of the weaker branch to the ppIII cycle, reduces the discrepancy between the SSM predictions and the ^{37}Cl results. This reduction does not resolve the solar neutrino problem because it also leads to an increase in the predicted ratio $\phi(^7\text{Be})/\phi(^8\text{B})$, exacerbating the most puzzling aspect of Equation (2).

Small differences between the Bahcall & Pinsonneault (BP) and Turck-Chièze & Lopez (TCL) calculations also exist in the low-energy extrapolation of the ^{3}He-^{3}He data of Krauss et al (1987). BP adopt the value of Parker & Rolfs (1991), who correct for small electron screening contributions that are believed to enhance the laboratory cross sections obtained at the lowest energies. The result is $S_{33}(0) = 5.0 \pm 0.3$ MeV b. TCL adopted the central value suggested by Assenbaum et al (1987) of 5.24 MeV b. The earlier Bahcall & Ulrich (1988) and Turck-Chièze et al calculations had used central values of 5.15 and 5.57 MeV b, respectively, the latter from a direct extrapolation of the Krauss et al data. The somewhat lower values adopted in the most recent calculations strengthen the branches to the ppII and ppIII cycles.

2.3 *Standard Solar Model Neutrino Fluxes*

There are some additional minor differences in the BP and TCL SSMs, e.g. in the solar lifetime, in $S_{34}(0)$, in the treatment of plasma effects on Thompson scattering, and in the composition. In addition, the BP calculation differs from that of TCL, and from those of the earlier Bahcall & Ulrich (1988; henceforth BU) SSM, by the inclusion of helium diffusion, which now is the largest contributor to the differences in the resulting flux predictions. The fluxes for the TCL and BP (with and without helium diffusion) SSMs are given in Table 1. It is reassuring that equivalent calculations (TCL and BP without helium diffusion) differ by less than 10% in their predictions of the temperature-dependent $\phi(^8\text{B})$. This flux is increased by 12% when helium diffusion is included.

Subsequent citations to the BP SSM refer to their model with helium diffusion. [Note added: Very recently the BP SSM has been updated by including heavy element diffusion (Bahcall & Pinsonneault 1995). The resulting ^{8}B neutrino flux is 6.62×10^6 cm^{-2}s^{-1}, an increase of 16% (31%) relative to the BP results with He diffusion (without diffusion) given in Table 1. The best value ^{37}Cl and ^{71}Ga capture rates are 9.3 and 137 SNU, respectively. The present-day helium surface value is 0.247, in good agreement with the helioseismology value of 0.242. The depth of the convective zone is also in excellent agreement with the value deduced from p-mode oscillation data.]

More important than the best values of the fluxes are the ranges that can be achieved by varying the parameters of the SSM within plausible bounds. To take into account the correlations among the fluxes when input parameters are varied, BU constructed 1000 SSMs by randomly varying five input parameters—the primordial heavy-element-to-hydrogen ratio Z/X and $S(0)$ for the p-p, and ^{3}He-^{3}He, ^{3}He-^{4}He, and p-^{7}Be reactions, assuming for each parameter a normal distribution with the mean and standard deviation used in their 1988 study. (These parameters were assigned the largest uncertainties.) Smaller uncertainties from radiative opacities, the solar luminosity, and the solar age were folded into the results of the model calculations perturbatively, by using the partial derivatives of the BU SSM (Bahcall & Haxton 1989).

The resulting pattern of ^{7}Be and ^{8}B flux predictions is shown in Figure 4. The elongated error ellipses indicate that the fluxes are strongly correlated. Those variations producing $\phi(^8\text{B})$ below $0.8\ \phi^{\text{SSM}}(^8\text{B})$ tend to produce a reduced $\phi(^7\text{Be})$, but the reduction is always less than 0.8. Thus a greatly reduced $\phi(^7\text{Be})$ cannot be achieved within the uncertainties assigned to parameters in the SSM.

A similar exploration, which included parameter variations very far from their preferred values, was carried out by Castellani et al (1994, 1995), who displayed

their results as a function of the resulting core temperature T_c. The pattern that emerges is striking (see Figure 5): Parameter variations producing the same value of T_c produce remarkably similar fluxes. Consequently, T_c provides an excellent one-parameter description of standard model perturbations. Figure 5 also illustrates the difficulty of producing a low ratio of $\phi(^7\text{Be})/\phi(^8\text{B})$ when T_c is reduced.

The BU 1000-solar-model variations were made under the constraint of reproducing the solar luminosity. Those variations show a similar strong correlation with T_c:

$$\phi(\text{pp}) \propto T_c^{-1.2}, \phi(^7\text{Be}) \propto T_c^{8}, \phi(^8\text{B}) \propto T_c^{18}. \quad (5)$$

Figures 4 and 5 are a compelling argument that reasonable variations in the parameters of the SSM, or nonstandard changes in quantities like the metallicity, opacities, or solar age, cannot produce the pattern of fluxes deduced from experiment (Equation 2). This would seem to limit possible solutions to errors

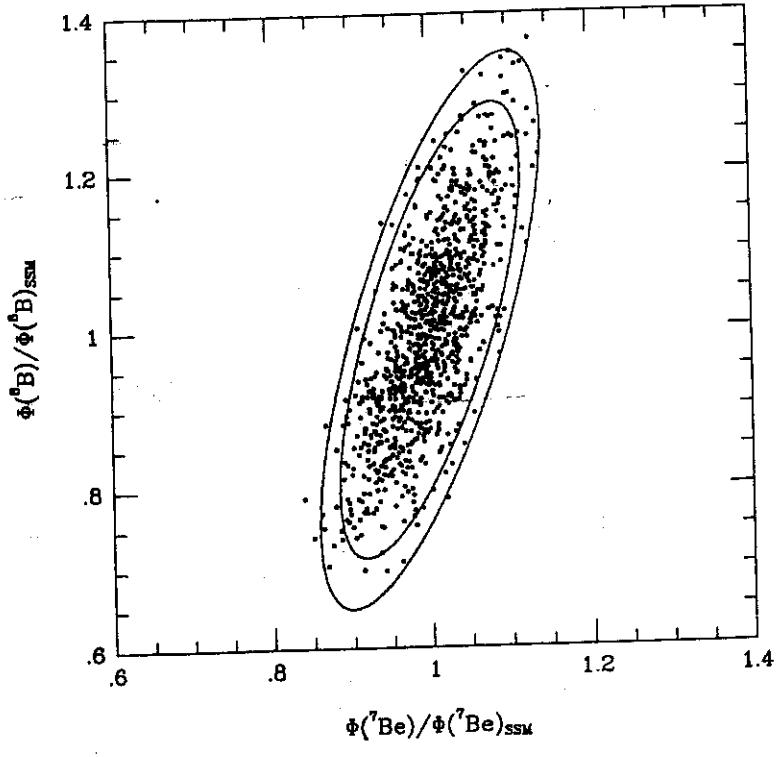

Figure 4 SSM ^{7}Be and ^{8}B flux predictions. The dots represent the fluxes resulting from the 1000 SSMs of Bahcall & Ulrich (1988), with smaller SSM uncertainties added as in Bahcall & Haxton (1989). The 90 and 99% confidence level error ellipses are shown.

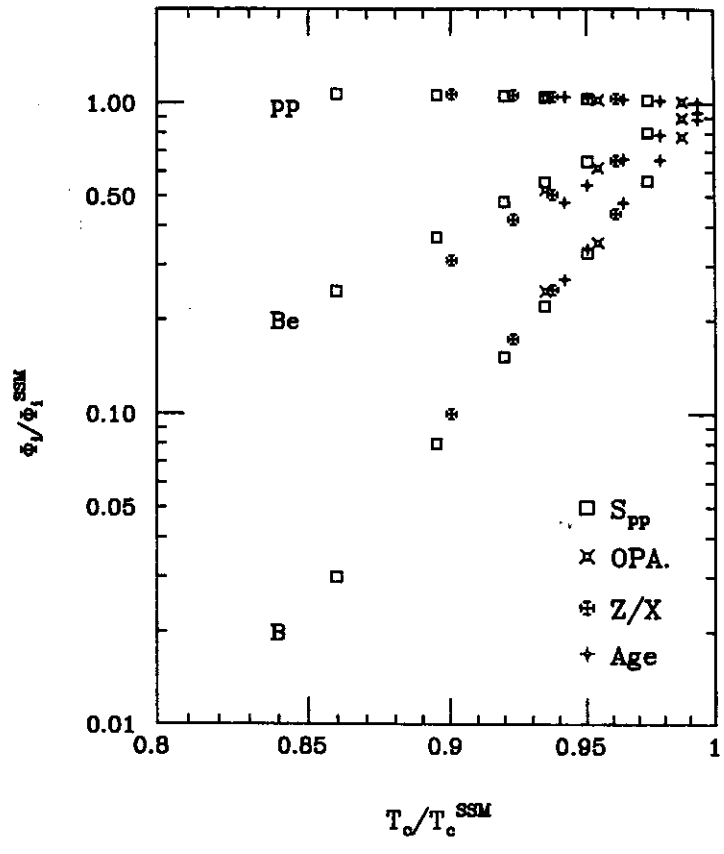

Figure 5 The response of the pp, Be, and ^{8}B fluxes to the indicated variations in solar model input parameters, displayed as a function of the resulting central temperature T_c. (From Castellani et al 1994.)

either in the underlying physics of the SSM or in our understanding of neutrino properties.

2.4 *Nonstandard Solar Models*

Nonstandard solar models include both variations of SSM parameters far outside the ranges generally believed to be reasonable (some examples of which are given in Figure 5) and changes in the underlying physics of the model. The solar neutrino problem has been a major stimulus to models of the second sort. However, there are other observations that suggest nonstandard processes could take place in the sun. The depletion of ^{7}Li in our sun (by a factor of 200) and in other solar-like stars is not understood. In a recent summary, Charbonnel (1995) argued that the depletion occurs on the main sequence after $\sim 10^8$

years and increases with time. The SSM predicts no solar lithium depletion: The base of the convective zone is too shallow to reach temperatures where lithium can be burned. While lithium depletion in lower mass stars ($\sim 0.9 M_\odot$) can be produced by lowering the low-temperature opacities, the depletion in heavier stars would seem to argue for diffusion or mixing mechanisms not yet incorporated into the SSM (Charbonnel 1995).

It is far from clear whether the lithium depletion problem will require changes in the SSM that will affect the deep, neutrino-producing regions of the sun. On the contrary, Charbonnel argues that the observed $^{12}C/^{13}C$ ratios in low-mass red giants requires a diffusion coefficient that decreases rapidly with depth.

Many nonstandard models were constructed to produce a reduction in T_c of about 5%, as this would have accounted for the low counting rate found in the Homestake experiment. The suggestions included models with low heavy element abundances ("low-Z" models), in which one abandons the SSM assumption that the initial heavy element abundances are those we measure today at the sun's surface; periodically mixed solar cores; models where hydrogen is continually mixed into the core by turbulent diffusion (Schatzman & Maeder 1981) or by convective mixing (Ezer & Cameron 1988, Shaviv & Salpeter 1968); and models where the solar core is partially supported by a strong central magnetic field (Abraham & Iben 1971, Bartenwerfer 1973, Parker 1974, Ulrich 1974) or by its rapid rotation (Demarque, Mengel & Sweigart 1973), thereby relaxing the SSM assumption that hydrostatic equilibrium is achieved only through the gas pressure gradient. A larger list is given by Bahcall & Davis (1982). To illustrate the kinds of consequences such models have, two of these suggestions are discussed in more detail below.

In low-Z models (Iben 1969, Bahcall & Ulrich 1971), one postulates a reduction in the core metallicity from $Z \sim 0.02$ to $Z \sim 0.002$. This lowers the core opacity (primarily because metals are very important to free-bound electron transitions), thus reducing T_c and weakening the ppII and ppIII cycles. The attractiveness of low-Z models is due in part to the existence of mechanisms for adding heavier elements to the sun's surface. These include the infall of comets and other debris, as well as the accumulation of dust as the sun passes through interstellar clouds. However, the increased radiative energy transport in low-Z models leads to a thin convective envelope, in contradiction to interpretations of the 5-min solar surface oscillations (Rhodes, Ulrich & Simon 1977; Christensen-Dalsgaard & Gough 1980). A low He mass fraction also results. Furthermore, Michaud (1977), noting that diffusion of material from a thin convective envelope into the interior would deplete heavy elements at the surface, questioned whether present abundances could have accumulated in low-Z models. Finally, the general consistency of solar heavy element abundances with those observed in other main sequence stars makes the model appear contrived.

Models in which the solar core ($\sim 0.2 M_\odot$) is intermittently mixed (Dilke & Gough 1972, Fowler 1972, Opik 1953) break the standard model assumption of a steady-state sun: For a period of several million years (approximately the Kelvin-Helmholtz time for the core) following mixing, the usual relationship between the observed surface luminosity and rate of energy (and neutrino) production is altered as the sun burns out of equilibrium. Calculations show that both the luminosity and the ^8B neutrino flux are suppressed while the sun relaxes back to the steady state.

Such models have been seriously considered because of instabilities associated with large gradients in the ^3He abundance. In the higher temperature central regions of the sun the pp chain reaches equilibrium quickly. The dominant ppI cycle production of ^3He is controlled by the p + p reaction rate, which varies as X^2T^4, where X and T are the local H mass fraction and temperature, respectively, while it is destroyed by the $^3He + {}^3He$ reaction at a rate proportional to $X_3^2 T^{16}$. Thus, the core ^3He abundance $X_3 \propto T^{-6}$ and rises steeply with increasing radius until a point where ^3He equilibrium has not yet been reached in the pp chain. This is approximately the peak of the ^3He abundance (at $r \sim 0.3\, r_\odot$ is the SSM): Beyond this point r the abundance declines quickly. (See Bahcall 1989, figure 4.2.) This profile is unstable under finite amplitude displacements of a volume to smaller r: The energy released by the increased ^3He burning at higher temperature can exceed the energy in the perturbation.

Dilke & Gough (1972), in the "solar spoon," proposed that the increased ^3He burning would also produce a linear instability of low-order, low-degree gravity modes, which they postulated could trigger large-scale mixing of the solar core. Under small oscillations, the enhanced burning in a volume element displaced downward increases the bouyant restoring force, leading to greater ascending velocities than descending ones. The question is whether this instability survives damping mechanisms such as radiative diffusion, turbulent convection, and couplings to higher-order g-modes. As Merryfield (1995) recently summarized, the possibility of an instability is still open, though no calculation has included all of the damping mechanisms thought to be important. He is far less optimistic about the possibility that the instability would drive large-scale, intermittent mixing (Merryfield, Toomre & Gough 1990). Theory suggests that the amplitude of such oscillations would saturate at velocities of ~ 10 km s^{-1}, but observation seems to rule out such large-amplitude, low-order, low-degree g-modes. The expected surface velocities of such modes would be comparable to the core velocities, exceeding the helioseismology bound of ~ 10 cm s^{-1} substantially.

These discussions of two of the more seriously explored nonstandard models illustrate how changes motivated by the solar neutrino problem often produce other unwanted consequences. Both examples underscore the growing

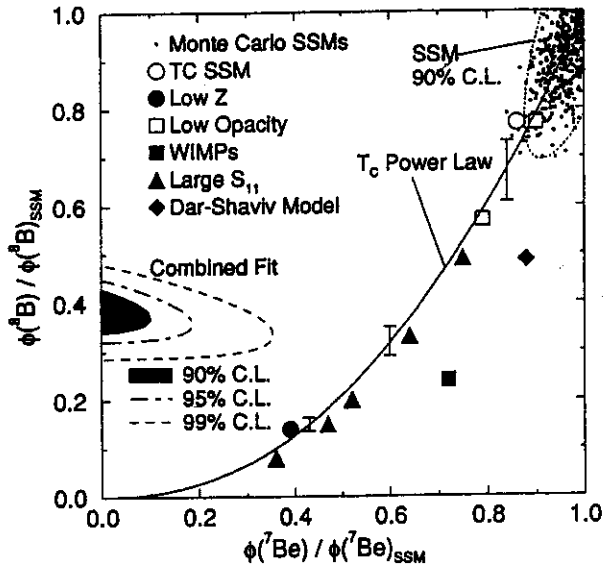

Figure 6 The fluxes allowed by the combined results of the Homestake, SAGE/GALLEX, and Kamiokande experiments compared to the results of SSM variations and various nonstandard models. The solid line is the T_c power law of Equation (3). (From Hata 1995.)

importance of helioseismology as a test of the SSM and as a constraint on its possible variations.

Figure 6 is an illustration by Hata (1995) of the flux predictions of several nonstandard models, including a low-Z model consistent with the ^{37}Cl results. As in the Castellani et al (1994) exploration, the results cluster along a track that defines the naive T_c dependence of the $\phi(^7\text{Be})/\phi(^8\text{B})$ ratio and are well separated from the experimental contours.

Of course, one cannot rule out a nonstandard solar model solution to the solar neutrino problem: The lack of success to date may merely reflect our lack of creativity. If such a model exists—one that is consistent with our general observations of main-sequence evolution of solar-type stars and with helioseismology—it likely involves some new and subtle physics.

3. THE DETECTION OF SOLAR NEUTRINOS

Four solar neutrino experiments have now provided data: the Homestake ^{37}Cl experiment, the gallium experiments SAGE and GALLEX, and Kamiokande. The first three detectors are radiochemical, while Kamiokande records neutrino-electron elastic scattering event-by-event.

3.1 *The Homestake Experiment*

Detection of neutrinos by the reaction $^{37}\text{Cl}(\nu_e,e)^{37}\text{Ar}$ was suggested independently by Pontecorvo (1946) and by Alvarez (1949). Davis's efforts to mount a 0.61-kiloton experiment using perchloroethylene (C_2Cl_4) were greatly helped by Bahcall's demonstration (1964a,b) that transitions to excited states in ^{37}Ar, particularly the superallowed transition to the analog state at 4.99 MeV, increased the ^{8}B cross section by a factor of 40. This suggested that Davis's detector would have the requisite sensitivity to detect ^{8}B neutrinos, thereby providing an accurate means of determining the central temperature of the sun. The experiment (see Figure 7) was mounted in the Homestake Gold Mine in Lead, South Dakota, in a cavity constructed approximately 4850 ft underground [4900 meters water equivalent (m.w.e.)]. It has operated continuously since 1967, apart from a 17-month hiatus in 1985–1986 caused by the failure of the circulation pumps. The result of 25 years of measurement is (Lande 1995)

$$\langle\sigma\phi\rangle_{^{37}\text{Cl}} = 2.55 \pm 0.17 \pm 0.18 \text{ SNU } (1\sigma), \tag{6}$$

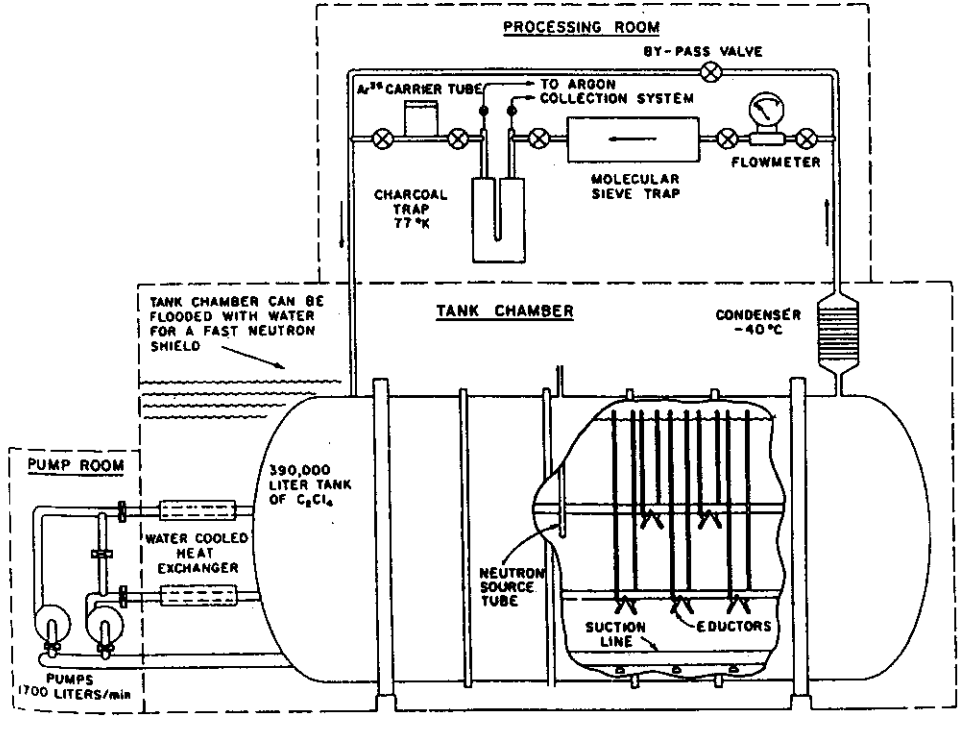

Figure 7 The Homestake ^{37}Cl solar neutrino experiment. This schematic is from the Davis, Harmer & Hoffman (1968) paper reporting the first results from their experiment.

which can be compared to the BP and TCL SSM predictions of 8.0 ± 1.0 SNU and 6.4 ± 1.4 SNU, respectively, all with 1σ errors. As we discuss below, the ^{8}B and ^{7}Be contributions account for 77% (73%) and 15% (17%), respectively, of the BP (TCL) total.

The experiment (Davis 1985, 1993) depends on the special properties of ^{37}Ar: As a noble gas, it can be removed readily from perchloroethylene, while its half-life ($\tau_{1/2} = 35$ days) allows both a reasonable exposure time and counting of the gas as it decays back to ^{37}Cl. Argon is removed from the tank by a helium purge, and the gas is then circulated through a condensor, a molecular sieve, and a charcoal trap cooled to the temperature of liquid nitrogen. Typically, ~95% of the argon in the tank is captured in the trap. (The efficiency is determined for each run from the recovery results for a known amount of carrier gas, ^{36}Ar or ^{38}Ar, introduced into the tank at the start of the run.) When the extraction is completed, the trap is heated and swept by helium. The extracted gas is passed through a hot titanium filter to remove reactive gases, and then other noble gases are separated by gas chromatography. The purified argon is loaded into a small proportional counter along with tritium-free methane, which serves as a counting gas. Because the electron capture decay of ^{37}Ar leads to the ground state of ^{37}Cl, the only signal for the decay is the 2.82 keV Auger electron produced as the atomic electrons in ^{37}Cl adjust to fill the K-shell vacancy. The counting of the gas typically continues for about one year (~10 half-lives).

The measured cosmic ray–induced background in the Homestake detector is 0.06 ^{37}Ar atoms/day; neutron-induced backgrounds are estimated to be below 0.03 atoms/day. A signal of 0.48 ± 0.04 atoms/day is attributed to solar neutrinos. When factors such as detector efficiencies, ^{37}Ar decays occurring in the tank, etc are taken into account, the number of ^{37}Ar atoms counted is about 25/year.

A variety of careful tests of the argon recovery and counting efficiency have been made over the past 25 years. For example, known amounts of ^{36}Cl were introduced into the tank in order to check the recovery of ^{36}Ar, with a resulting yield of $100 \pm 3\%$. It has also been verified that ^{37}Ar produced in the tank by a fast neutron source, which induces (n,p) reactions followed by (p,n) on ^{37}Cl, is quantitatively recovered. However, the detector has never been calibrated directly with a neutrino source, despite studies of the feasibility of using a ^{65}Zn source (Alvarez 1973).

The significance of the Homestake results is due in part to an accurately determined ^{37}Cl cross section. As the 814 keV threshold for exciting the ^{37}Ar ground state is above the pp endpoint, the detector is sensitive primarily to ^{7}Be and ^{8}B neutrinos (see Table 2). The cross section for ^{7}Be neutrinos (and the weaker fluxes of pep and CNO cycle neutrinos) is determined by the known half-life of ^{37}Ar. However, ^{8}B neutrinos can generate transitions to many excited states below the particle breakup threshold in ^{37}Ar. The superallowed

Table 2 Predicted capture rates in SNU of the BP and TCL SSMs for the ^{37}Cl and SAGE/GALLEX experiments

	capture rates			
Neutrino source	^{37}Cl(BP)	^{37}Cl(TCL)	^{71}Ga(BP)	^{71}Ga(TCL)
pp	0.0	0.0	70.8	71.1
pep	0.2	0.22	3.1	2.99
^{7}Be	1.2	1.10	35.8	30.9
^{8}B	6.2	4.63	13.8	10.77
^{13}N	0.1	0.063	3.0	2.36
^{15}O	0.3	0.21	4.9	3.66
Total	8.0	6.36	131.5	122.5

transition to the 4.99 MeV state, dominated by the Fermi matrix element of known strength, accounts for about 60% of the SSM cross section. The allowed transition strengths can be measured by observing the delayed protons following the β decay of ^{37}Ca, the isospin analog of the reaction ^{37}Cl(ν_e,e) ^{37}Ar (Bahcall 1966). Although it was believed that this measurement had been properly done many years ago (Poskanzer et al 1966; Sextro, Gough & Cerny 1974), the issue was not resolved until kinematically complete measurements were recently made (Garcia et al 1991, 1995; Adelberger & Haxton 1987). The net result is a ^{37}Cl cross section believed to be accurate to about 3%.

3.2 *The Kamiokande Experiment*

The Kamiokande experiment (Hirata et al 1988, 1991) is a 4.5-kiloton cylindrical imaging water Cerenkov detector originally designed for proton decay searches, but later reinstrumented to detect low-energy neutrinos. It detects neutrinos by the Cerenkov light produced by recoiling electrons in the reaction

$$\nu_x + e \rightarrow \nu_x' + e'. \tag{7}$$

Both ν_e and heavy flavor neutrinos contribute, with $\sigma(\nu_e)/\sigma(\nu_\mu) \sim 7$. The inner volume of 2.14 kilotons is viewed by 948 Hamamatsu 20″ photomultiplier tubes (PMTs), which provide 20% photocathode coverage, and the surrounding 1.5 m of water, serving as an anticounter, is viewed by 123 PMTs. The fiducial volume for solar neutrino measurements is the central 0.68 kilotons of water, the detector region most isolated from the high-energy gamma rays generated in the surrounding rock walls of the Kamioka mine.

In the conversion of the original proton decay detector to Kamiokande II, great effort was invested in reducing low-energy backgrounds associated with radon and uranium. This included sealing the detector against radon inleakage and recirculating the water through ion exchange columns. The relatively shallow depth of the Kamioka mine (2700 m.w.e.) leads to an appreciable flux of cosmic-ray muons, which, on interacting with ^{16}O, produce various

short-lived spallation products. These β decay activities are vetoed by their correlation in time with the muons. The experimenters succeeded in lowering the detector threshold to 9 MeV and later to 7.5 MeV. Kamiokande III included improvements in the electronics and the installation of wavelength shifters around the PMTs to increase light collection and currently operates with a threshold of 7.0 MeV.

Kamiokande II/III detects the high-energy portion of the ^{8}B neutrino spectrum. Between December 1985 and July 1993, 1667 live detector days of data were accumulated. Under the assumption that the incident neutrinos are ν_es with an undistorted ^{8}B β decay spectrum, the combined Kamiokande II/III data set gives (Suzuki 1995, Nakamura 1994)

$$\phi_{\nu_e}(^8\mathrm{B}) = (2.89 \pm 0.22 \pm 0.35) \cdot 10^6 \mathrm{cm}^{-2}\,\mathrm{s}^{-1}(1\sigma). \quad (8)$$

This corresponds to 51% of the BP and 63% of the TCL SSM predictions. The total number of detected solar neutrino events is 476^{+36}_{-34}.

This experiment is remarkable in several respects. It is the first detector to measure solar neutrinos in real time. Essential to the experiment is the sharp peaking of the electron angular distribution in the direction of the incident neutrino: This forward peaking, illustrated in Figure 8, allows the experimenters to separate solar neutrino events from an isotropic background. The unambiguous observation of a peak in the cross section correlated with the position of the sun is the first direct demonstration that the sun produces neutrinos as a byproduct

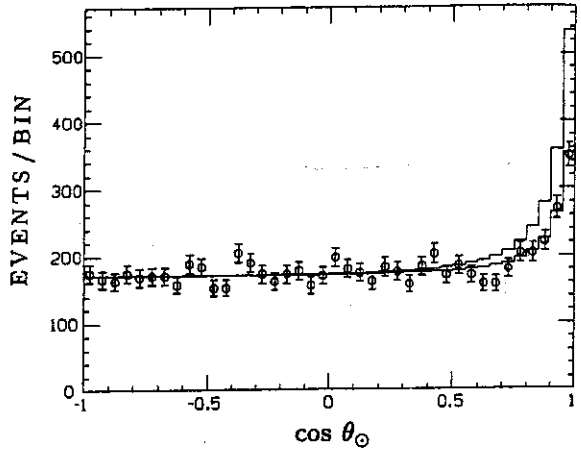

Figure 8 Angular distribution of recoil electrons from Kamiokande II and III showing the excess at forward angles that is attributed to solar neutrinos. Electrons with apparent energies between 7 and 20 MeV are included. The upper histogram is the SSM prediction of Bahcall & Ulrich (1988) superimposed on an isotropic background, while the lower histogram is the best fit. (From Nakamura 1994.)

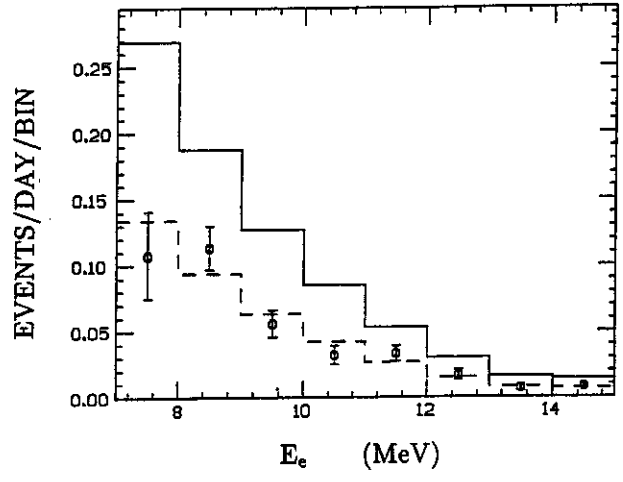

Figure 9 The Kamiokande II/III recoil electron energy spectrum compared to the SSM prediction (*solid histogram*) and to the SSM prediction rescaled by a factor of 0.5 (*dashed histogram*). The last bin corresponds to apparent electron energies between 14 and 20 MeV. (From Nakamura 1994.)

of fusion. Finally, although Reaction (7) is a soft process in which the recoil electron and scattered neutrino share the initial energy, the recoil electron energy distribution provides some information on the incident neutrino spectrum. The recoil spectrum measured by Kamiokande II/III, shown in Figure 9, is consistent with an allowed ^{8}B incident neutrino spectrum, with the overall flux reduced as in Equation (8).

3.3 *The SAGE and GALLEX Experiments*

Two radiochemical gallium experiments exploiting the reaction $^{71}\mathrm{Ga}(\nu_e,\mathrm{e})^{71}\mathrm{Ge}$, SAGE and GALLEX, began solar neutrino measurements in January 1990 and May 1991, respectively. SAGE operates in the Baksan Neutrino Observatory, under 4700 m.w.e. of shielding from Mount Andyrchi in the Caucasus, while GALLEX is housed in the Gran Sasso Laboratory in Italy at a depth of 3300 m.w.e. These experiments are sensitive primarily to the low-energy pp neutrinos, the flux of which is sharply constrained by the solar luminosity in any steady-state model of the sun (see Table 2). The gallium experiment was first suggested by Kuzmin (1966). In 1974 Ray Davis and collaborators began work to develop a practical experimental scheme. Their efforts, in which both $GaCl_3$ solutions and Ga metal targets were explored, culminated with the 1.3-ton Brookhaven/Heidelberg/Rehovot/Princeton pilot experiment in 1980–1982 that demonstrated the procedures later used by GALLEX (Hampel 1985).

The primary obstacles to mounting the gallium experiments were the cost of the target and the greater complexity of the ^{71}Ge chemical extraction. The

GALLEX experiment (Anselmann et al 1992, 1994a) employs 30 tons of Ga as a solution of $GaCl_3$ in hydrochloric acid. After an exposure of about three weeks, the germanium is recovered as $GeCl_4$ by bubbling nitrogen through the solution and then scrubbing the gas through a water absorber. The Ge is further concentrated and purified, and finally converted into GeH_4 which, when mixed with Xe, makes a good counting gas. The overall extraction efficiency is typically 99%. The GeH_4 is inserted into miniaturized gas proportional counters, carefully designed for their radiopurity, and the Ge is counted as it decays back to Ga ($\tau_{1/2} = 11.43$ d). As in the case of ^{37}Ar, the only signal for the Ge decay is the energy deposited by Auger electrons and X rays that accompany the atomic rearrangement in Ga. An important achievement of GALLEX has been the detection of both the K peak (10.4 keV) and L peak (1.2 keV). While 88% of the electron captures occur from the K shell, many of the subsequent K $\rightarrow$ L X rays escape the detector and some of the Auger electrons hit the detector walls. This produces a shift of the detected energy of events from the K to the L and M peaks. Thus the GALLEX L-peak counting capability almost doubles the ^{71}Ge detection efficiency.

Gallium, like mercury, is a liquid metal at room temperature. SAGE (Abdurashitov et al 1994, Bowles & Gavrin 1993) uses metallic gallium as a target; the ^{71}Ge is separated by vigorously mixing into the gallium a mixture of hydrogen peroxide and dilute hydrochloric acid. This produces an emulsion, with the Ge migrating to the surface of the emulsion droplets where it is oxidized and dissolved by hydrochloric acid. The Ge is extracted as $GeCl_4$, purified and concentrated, synthesized into GeH_4, and further purified by gas chromatography. The overall efficiency, determined by introducing a Ge carrier, is typically 80%. The Ge counting proceeds as in GALLEX. SAGE began operations with 30 tons of gallium, and now operates with 55 tons. The combined result for stage I (prior to September 1992) and the first nine runs of stage II (September 1992 to June 1993) is (Nico 1995)

$$\langle \sigma\phi \rangle_{^{71}Ge} = 69^{+11}_{-11}\,(\text{stat})^{+5}_{-7}\,(\text{sys})\ \text{SNU}(1\sigma). \tag{9}$$

This result includes only events counted in the K peak. The counter and electronics improvements made at the start of stage II should permit L-peak events to be included, but no results have been announced as of December 1994. The corresponding results for GALLEX I (first 15 runs) and II (August 1992 to October 1993) is (Anselmann et al 1994)

$$\langle \sigma\phi \rangle_{^{71}Ge} = 79 \pm 10 \pm 6\ \text{SNU}(1\sigma). \tag{10}$$

GALLEX II solar neutrino runs continued until June 1994, but results for the last portion of this period have not been reported.

GALLEX II solar neutrino runs were interrupted in June 1994 to permit an overall test of the detector with a ^{51}Cr source, which produces line sources

of 746 keV (90%) and 426 keV (10%) neutrinos. The 1.67 MCi source was produced by irradiating ~36 kg of chromium, enriched in ^{50}Cr, in the Siloé reactor in Grenoble. Following exposure of the detector and recovery and counting of the produced ^{71}Ge, the ratio of measured ^{71}Ge to expected was calculated (Anselmann et al 1995),

$$R = 1.04 \pm 0.12(1\sigma). \tag{11}$$

This is the first test of a solar neutrino detector with an terrestrial, low-energy neutrino source. A similar source (~0.5 MCi) has been produced by the SAGE collaboration and was installed in their detector in December 1994 (JF Wilkerson, private communication). At the time this review was written (March 1995), five of approximately eight planned extractions had been completed in the source experiment. The ^{71}Ge counting was proceeding routinely, and an announcement of the results is expected later this year. The higher Ga density of the SAGE detector increases the effectiveness of the source by about a factor of 2.5, helping to compensate for the weaker neutrino flux.

The nuclear physics of the reaction $^{71}Ga(\nu_e,e)^{71}Ge$ is illustrated in Figure 10. As the threshold is 233 keV, the ground state and first excited state can be excited by pp neutrinos. However, as only those pp neutrinos within 12 keV of the endpoint can reach the excited state, the phase space for reaching this state is smaller by a factor of ~100. Thus, the cross section is determined precisely by the measured electron capture lifetime of ^{71}Ge. In the BP and TCL calculations

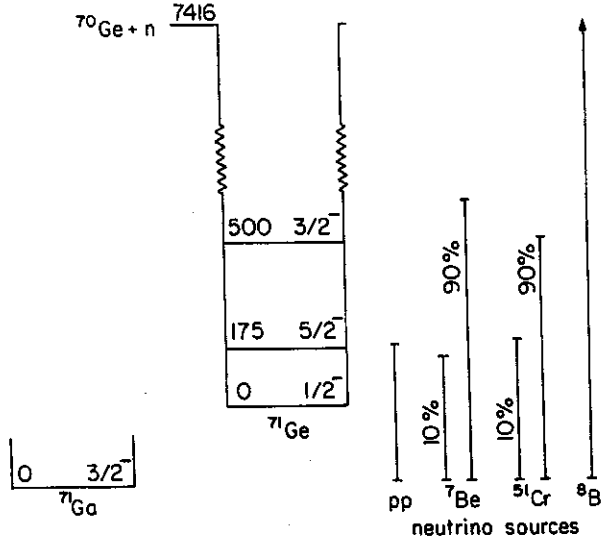

Figure 10 Level scheme for ^{71}Ge showing the excited states that contribute to absorption of pp, ^{7}Be, ^{51}Cr, and ^{8}B neutrinos. The $^{70}Ge + n$ break-up threshold is 7.4 MeV.

these neutrinos account for 54 and 57% of the capture rate, respectively, each predicting 71 SNU. Because of this strong pp neutrino contribution, there exists a minimal astronomical counting rate of 79 SNU (Bahcall 1989) for the Ga detector that assumes only a steady-state sun and standard model weak interaction physics. This minimum value corresponds to a sun that produces the observed luminosity entirely through the ppI cycle. The rates found by SAGE and GALLEX are quite close to this bound.

The ^{7}Be neutrinos can excite the ground state and two excited states at 175 keV ($5/2^-$) and 500 keV ($3/2^-$). The SSM rates quoted above assume that these excited state transitions are much weaker than the ground-state transition, contributing only 5% to the ^{7}Be rate. The primary justification for this is the forward-angle (p,n) calibration of Gamow-Teller (GT) transitions to these states by Krofcheck et al (1985). However, although the track record of (p,n) mappings of the broad features of the Gamow-Teller resonance is quite good, the technique is not generally considered a reliable test of the GT strength carried by an isolated state unless the transition to that state is quite strong (Austin et al 1994). On the other hand, all three ^{7}Be transitions are tested in the ^{51}Cr calibration, where they are weighted by phase space factors quite similar to those of ^{7}Be neutrinos (Haxton 1988a). Given other checks the GALLEX collaboration has made of the detector's overall chemical efficiency, another interpretation (Hata & Haxton 1995) of the source experiment is that it verifies that the excited states play a minor role in the ^{7}Be capture rate. As the SSM ^{7}Be capture rates of BP and TCL are both above 30 SNU, the SAGE/GALLEX results alone suggest some reduction in the low-energy pp and/or ^{7}Be fluxes.

The ^{8}B neutrino capture rates (14 and 11 SNU in the BP and TCL SSMs, respectively) have been calculated from the GT profile deduced by Krofcheck et al (1985). The corresponding total SSM rates for this detector are 132 SNU and 123 SNU (see Table 2).

3.4 *The Molybdenum Experiment*

Recently, an effort was made to do a solar neutrino experiment of a different kind: a geochemical integration of the ^{8}B neutrino flux over the past several million years (Cowan & Haxton 1982, Wolfsberg et al 1985). The reaction

$$\nu_e + {}^{98}\mathrm{Mo} \rightarrow e^- + {}^{98}\mathrm{Tc}\ (\tau_{1/2} = 4.2 \cdot 10^6\ \mathrm{y}) \qquad (12)$$

occurring over geologic times can produce concentrations of ^{98}Tc of ~ 10 atoms per gram of ^{98}Mo (abundance 24%). Because no stable isotopes of technetium exist, such a concentration is, in principle, measureable. Careful calculations of backgrounds from natural radioactivity and cosmic rays indicated that these would be tolerable in a deeply buried ore body.

The motivation of the experiment differs from others we have discussed: A comparison of ^{8}B flux averaged over an appreciable fraction of the Kelvin-Helmholtz time with contemporary measurements would test the long-term thermal stability of the core.

The challenge is to isolate and quantitatively count $\sim 10^8$ atoms of ^{98}Tc from 2600 tons of raw ore (containing 13 tons of molybdenum) obtained from the one operating deep mine in North America—the Henderson Mine in Clear Creek County, Colorado. Two major tasks faced the experimenters: isolating the Tc from this enormous quantity of ore and doing quantitative Tc mass spectrometry at the required accuracy level. The first goal appeared reachable as it is known that chemically analogous rhenium can be quantitatively recovered from the gas stream of commercial molybdenum roasters. The second goal was reached after several years of work.

The experiment was mounted by Los Alamos National Laboratory with the help of the AMAX Mining Corporation. The experimenters achieved a sensitivity to Tc at about the 100 SNU level, five times the expected SSM production rate. At that level a background appeared due to the commercial roaster's "memory" of recently roasted molybdenum from shallow mines in which cosmic ray–induced Tc levels are high. Although the plant memory decays with time, the necessary flushing of the roaster with several weeks of Henderson ore was not practical commercially. The effort was abandoned in 1988.

Apparently, this experiment must await a factor of 10–100 further improvement in Tc mass spectrometry. At this sensitivity, the roasting of the MoS_2 concentrate could be done under controlled laboratory conditions on a "tabletop" scale of 10–100 kg.

4. PARTICLE PHYSICS SOLUTIONS

In Section 2 it was shown that solar models that reduce the high-energy neutrino flux tend to enhance the ^{7}Be/^{8}B flux ratio, contradicting the results of the Homestake, SAGE/GALLEX, and Kamiokande experiments.

If the source of the solar neutrino problem is not solar, the remaining possibilities are experimental error or nonstandard particle physics. Several researchers have recently considered the consequences of ignoring one of the three experiments just discussed (Parke 1995, Bahcall 1994, Kwong & Rosen 1994, Bahcall & Bethe 1990). Substantial discrepancies between SSM predictions and the remaining experiments persist. For example, Figure 11 shows Parke's results when only the Kamiokande and SAGE/GALLEX constraints are retained: A discrepancy of almost 3–4 σ remains, depending on the choice of SSM. The corresponding results for other combinations show even larger inconsistencies. If two experiments must be flawed to account for the discrepancy with the SSM, this scenario becomes somewhat less credible.

The second alternative—physics beyond the standard model of electroweak interactions—would have the most far-reaching consequences. Particle physics solutions of the solar neutrino problem include neutrino oscillations, neutrino

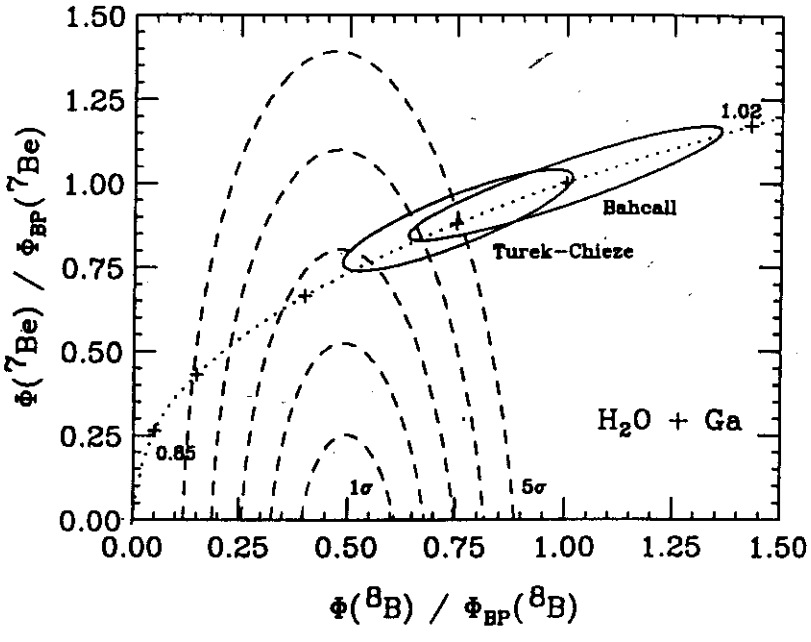

Figure 11 The ^{7}Be and ^{8}B fluxes determined by the SAGE/GALLEX and Kamiokande experiments compared to the predictions of the BP and TCL SSMs. (From Parke 1994.)

decay, neutrino magnetic moments, and weakly interacting massive particles. Among these, the Mikheyev-Smirnov-Wolfenstein effect—neutrino oscillations enhanced by matter interactions—is widely regarded as the most plausible.

4.1 *Neutrino Masses and Vacuum Oscillations*

One odd feature of particle physics is that neutrinos, which are not required by any symmetry to be massless, nevertheless must be much lighter than any of the other known fermions. For instance, the current limit on the ν_e mass is $\lesssim 5$ eV. The standard model requires neutrinos to be massless, but the reasons are not fundamental. Dirac mass terms m_D, analogous to the mass terms for other fermions, cannot be constructed because the model contains no right-handed neutrino fields.

Neutrinos can also have Majorana mass terms

$$\overline{\nu_L^c} m_L \nu_L$$

and

$$\overline{\nu_R^c} m_R \nu_R, \tag{13}$$

where the subscripts L and R refer to left- and right-handed projections of the neutrino field ν and the superscript c denotes charge conjugation. The first of these contains left-handed fields, but can only arise as a nonrenormalizable effective interaction when one is constrained to generate m_L with the doublet scalar field of the standard model. The second term is absent from the standard model because there are no right-handed neutrino fields.

None of these standard model arguments carries over to the more general, unified theories that theorists believe will supplant the standard model. In the enlarged multiplets of extended models it is natural to characterize the fermions of a single family, e.g. ν_e, e, u, d, by the same mass scale m_D. Small neutrino masses are then frequently explained as a result of the Majorana neutrino masses. In the seesaw mechanism,

$$M_\nu \sim \begin{pmatrix} 0 & m_D \\ m_D^T & m_R \end{pmatrix}. \tag{14}$$

Diagonalization of the mass matrix produces one light neutrino, $m_{\text{light}} \sim (m_D^2)/(m_R)$, and one unobservably heavy neutrino, $m_{\text{heavy}} \sim m_R$. The factor (m_D/m_R) is the needed small parameter that accounts for the distinct scale of neutrino masses. The masses for the ν_e, ν_μ, and ν_τ are then related to the squares of the corresponding quark masses m_u, m_c, and m_t. Taking $m_R \sim 10^{16}$ GeV, a typical grand unification scale for models built on groups like SO(10), the seesaw mechanism gives the crude relation

$$m_{\nu_e} : m_{\nu_\mu} : m_{\nu_\tau} \leftrightarrow 2 \cdot 10^{-12} : 2 \cdot 10^{-7} : 3 \cdot 10^{-3}\ \text{eV}. \tag{15}$$

The fact that solar neutrino experiments can probe small neutrino masses, and thus provide insight into possible new mass scales m_R that are far beyond the reach of direct accelerator measurements, has been an important theme of the field (Babu & Mohapatra 1993; Bludman, Kennedy & Langacker 1992; Dimopoulos, Hall & Raby 1993).

Another expectation is that neutrinos from the different families mix, just as quark mixing is observed in hyperon and nucleon β decays. If we consider the two-flavor case for simplicity, the mass eigenstates $|\nu_1\rangle$ and $|\nu_2\rangle$ (with masses m_1 and m_2) are related to the weak interaction eigenstates by

$$\begin{aligned} |\nu_e\rangle &= \cos\theta_v |\nu_1\rangle + \sin\theta_v |\nu_2\rangle, \\ |\nu_\mu\rangle &= -\sin\theta_v |\nu_1\rangle + \cos\theta_v |\nu_2\rangle, \end{aligned} \tag{16}$$

where θ_v is the (vacuum) mixing angle. The two mass eigenstates comprising the ν_e then propagate with different phases in vacuum, leading to flavor oscillations. The probability that a ν_e will remain a ν_e after propagating a distance x is

$$P_{\nu_e}(x) = 1 - \sin^2 2\theta_v \sin^2\left(\frac{\delta m^2 x}{4E}\right) \underset{x\to\infty}{\to} 1 - \frac{1}{2}\sin^2 2\theta_v, \tag{17}$$

where E is the neutrino energy and $\delta m^2 = m_2^2 - m_1^2$. (When one properly describes the neutrino state as a wave packet, the large-distance behavior follows

from the eventual separation of the mass eigenstates.) If the the oscillation length

$$L_0 = \frac{4\pi E}{\delta m^2} \tag{18}$$

is comparable to or shorter than one astronomical unit, a reduction in the ν_e flux would be expected in terrestrial neutrino oscillations. The suggestion that the solar neutrino problem could be explained by neutrino oscillations was first made by Pontecorvo (1958), who pointed out the analogy with $K_0 \leftrightarrow \bar{K}_0$ oscillations. From the point of view of particle physics, the sun is a marvelous neutrino source. The neutrinos travel a long distance and have low energies ($\sim$ 1 MeV), implying a sensitivity to

$$\delta m^2 \gtrsim 10^{-12}\,\mathrm{eV}^2. \tag{19}$$

In the seesaw mechanism, $\delta m^2 \sim m_2^2$, so neutrino masses as low as $m_2 \sim 10^{-6}$ eV could be probed. In contrast, terrestrial oscillation experiments with accelerator or reactor neutrinos are typically limited to $\delta m^2 \gtrsim 0.1\ \mathrm{eV}^2$.

From Equation (17) one expects vacuum oscillations to affect all neutrino species equally if the oscillation length is small compared to an astronomical unit. This appears to contradict observation, as the pp flux may not be significantly reduced. Furthermore, the theoretical prejudice that θ_v should be small makes this an unlikely explanation of the significant discrepancies with SSM ^{7}Be and ^{8}B flux predictions.

The first objection, however, can be circumvented in the case of "just so" oscillations where the oscillation length is comparable to one astronomical unit (Glashow & Krauss 1987). In this case the oscillation probability becomes sharply energy dependent, and one can choose δm^2 to preferentially suppress one component (e.g. the monochromatic ^{7}Be neutrinos). This scenario has been explored by several groups and remains an interesting possibility. However, large mixing angles are still required.

4.2 *The Mikheyev-Smirnov-Wolfenstein Mechanism*

The community's view of neutrino oscillations changed radically when Mikheyev & Smirnov (1985, 1986) showed that the density dependence of the neutrino effective mass, a phenomenon first discussed by Wolfenstein (1978), could greatly enhance oscillation probabilities: A ν_e is adiabatically transformed into a ν_μ as it traverses a critical density within the sun. It became clear that the sun was not only an excellent neutrino source, but also a natural regenerator for cleverly enhancing the effects of flavor mixing.

Although the original work of Mikheyev & Smirnov was numerical, their phenomenon was soon understood analytically as a level-crossing problem. If one writes the neutrino wave function in matter as

$$|\nu(x)\rangle = a_e(x)|\nu_e\rangle + a_\mu(x)|\nu_\mu\rangle,$$

where x is the coordinate along the neutrino's path, the evolution of $a_e(x)$ and $a_\mu(x)$ is governed by

$$i\frac{d}{dx}\begin{pmatrix} a_e \\ a_\mu \end{pmatrix} = \frac{1}{4E} \times \tag{20}$$

$$\begin{pmatrix} 2E\sqrt{2}G_F\rho(x) - \delta m^2\cos 2\theta_v & \delta m^2 \sin 2\theta_v \\ \delta m^2 \sin 2\theta_v & -2E\sqrt{2}G_F\rho(x) + \delta m^2 \cos 2\theta_v \end{pmatrix}\begin{pmatrix} a_e \\ a_\mu \end{pmatrix},$$

where G_F is the weak coupling constant and $\rho(x)$ is the solar electron density. If $\rho(x) = 0$, Equation (20) can be trivially integrated to give the vacuum oscillation solution (Equation 17). The new contribution to the diagonal elements, $2E\sqrt{2}G_F\rho(x)$, represents the effective contribution to M_ν^2 that arises from neutrino-electron scattering. The indices of refraction of electron and muon neutrinos differ because the former scatter by charged and neutral currents, while the latter have only neutral current interactions. The difference in the forward scattering amplitudes determines the density-dependent splitting of the diagonal elements of Equation (20).

It is helpful to rewrite Equation (20) in a basis consisting of the light (L) and heavy (H) local mass eigenstates [i.e. the states that diagonalize the right-hand side of Equation (20)],

$$\begin{aligned} |\nu_L(x)\rangle &= \cos\theta(x)|\nu_e\rangle - \sin\theta(x)|\nu_\mu\rangle, \\ |\nu_H(x)\rangle &= \sin\theta(x)|\nu_e\rangle + \cos\theta(x)|\nu_\mu\rangle. \end{aligned} \tag{21}$$

The local mixing angle is defined by

$$\begin{aligned} \sin 2\theta(x) &= \frac{\sin 2\theta_v}{\sqrt{X^2(x) + \sin^2 2\theta_v}}, \\ \cos 2\theta(x) &= \frac{-X(x)}{\sqrt{X^2(x) + \sin^2 2\theta_v}}, \end{aligned} \tag{22}$$

where $X(x) = 2\sqrt{2}G_F\rho(x)E/\delta m^2 - \cos 2\theta_v$. Thus $\theta(x)$ ranges from θ_v to $\pi/2$ as the density $\rho(x)$ goes from 0 to ∞.

If we define

$$|\nu(x)\rangle = a_H(x)|\nu_H(x)\rangle + a_L(x)|\nu_L(x)\rangle,$$

Equation (20) becomes

$$i\frac{d}{dx}\begin{pmatrix} a_H \\ a_L \end{pmatrix} = \begin{pmatrix} \lambda(x) & i\alpha(x) \\ -i\alpha(x) & -\lambda(x) \end{pmatrix}\begin{pmatrix} a_H \\ a_L \end{pmatrix}, \tag{23}$$

with the splitting of the local mass eigenstates determined by

$$2\lambda(x) = \frac{\delta m^2}{2E}\sqrt{X^2(x) + \sin^2 2\theta_v} \tag{24}$$

and with mixing of these eigenstates governed by the density gradient

$$\alpha(x) = \left(\frac{E}{\delta m^2}\right)\frac{\sqrt{2}\,G_F\frac{d}{dx}\rho(x)\sin 2\theta_v}{X^2(x)+\sin^2 2\theta_v}. \tag{25}$$

Note that the splitting achieves its minimum value,

$$\frac{\delta m^2}{2E}\sin 2\theta_v,$$

at a critical density $\rho_c = \rho(x_c)$ that defines the point where the diagonal elements of Equation (20) cross:

$$2\sqrt{2}EG_F\rho_c = \delta m^2 \cos 2\theta_v. \tag{26}$$

Equation (23) can be trivially integrated if the splitting of the diagonal elements is large compared to the off-diagonal elements,

$$\gamma(x) = \left|\frac{\lambda(x)}{\alpha(x)}\right|$$

$$= \frac{\sin^2 2\theta_v}{\cos 2\theta_v}\frac{\delta m^2}{2E}\frac{1}{\left|\frac{1}{\rho_c}\frac{d\rho(x)}{dx}\right|}\frac{\left[X(x)^2+\sin^2 2\theta_v\right]^{3/2}}{\sin^3 2\theta_v} \gg 1, \tag{27}$$

a condition that becomes particularly stringent near the crossing point,

$$\gamma_c = \gamma(x_c) = \frac{\sin^2 2\theta_v}{\cos 2\theta_v}\frac{\delta m^2}{2E}\frac{1}{\left|\frac{1}{\rho_c}\frac{d\rho(x)}{dx}\right|_{x=x_c}} \gg 1. \tag{28}$$

The resulting adiabatic electron neutrino survival probability, valid when $\gamma_c \gg 1$, is

$$P_{\nu_e}^{\text{adiab}} = \frac{1}{2} + \frac{1}{2}\cos 2\theta_v \cos 2\theta_i, \tag{29}$$

where $\theta_i = \theta(x_i)$ is the local mixing angle at the density where the neutrino was produced. Equation (29) was first discussed by Bethe (1986) (also see Messiah 1986).

The physical picture behind this derivation is illustrated in Figure 12. One makes the usual assumption that, in vacuum, the ν_e is almost identical to the light mass eigenstate, $\nu_L(0)$, i.e. $m_1 < m_2$ and $\cos\theta_v \sim 1$. However, as the density increases, the matter effects make the ν_e heavier than the ν_μ, with $\nu_e \to \nu_H(x)$ as $\rho(x)$ becomes large. The special property of the sun is that it produces ν_es at high density that then propagate to the vacuum where they are measured. The adiabatic approximation tells us that if initially $\nu_e \sim \nu_H(x)$, the neutrino will remain on the heavy mass trajectory provided the density changes slowly. That

is, if the solar density gradient is sufficiently gentle, the neutrino will emerge from the sun as the heavy vacuum eigenstate, $\nu_H(0) \sim \nu_\mu$. This guarantees nearly complete conversion of ν_es into ν_μs, producing a flux that cannot be detected by the Homestake or SAGE/GALLEX detectors.

This physical picture does not, however, explain the curious pattern of partial flux suppressions of Equation (2). The key to this pattern is the behavior when $\gamma_c \lesssim 1$. Equations (28) and (29) show that the critical region for nonadiabatic behavior occurs in a narrow region (for small θ_v) surrounding the crossing point and that this behavior is controlled by the derivative of the density. This relationship permits an analytic strategy for handling nonadiabatic crossings: One can replace the true solar density by a simpler (integrable!) two-parameter form that is constrained to reproduce the true density and its derivative at the crossing point x_c. Two convenient choices are the linear $[\rho(x) = a + bx]$ and exponential $[\rho(x) = a\exp(-bx)]$ profiles. As the density derivative at x_c governs the nonadiabatic behavior, this procedure should provide an accurate description of the hopping probability between the local mass eigenstates when the neutrino traverses the crossing point. The initial and ending points, x_i and x_f, for the artificial profile are then chosen so that $\rho(x_i)$ is the density where the neutrino was produced in the solar core and $\rho(x_f) = 0$ (the solar surface), as illustrated in Figure 13. Because the adiabatic result (Equation 29) depends only on the local mixing angles at these points, this choice builds in that limit. Equation (20) can then be integrated exactly for linear and exponential profiles, with the results given in terms of parabolic cylinder and Whittaker

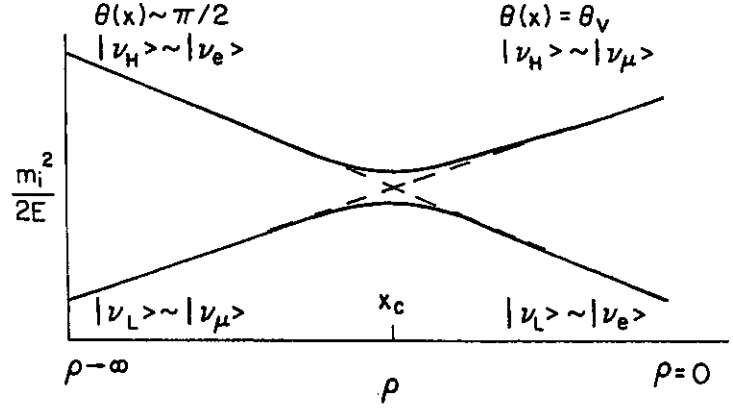

Figure 12 Schematic illustration of the MSW level crossing. The dashed lines correspond to the electron-electron and muon-muon diagonal elements of the matrix in Equation (20). Their intersection defines the level-crossing density ρ_c. The solid lines are the trajectories of the light and heavy local mass eigenstates. If the electron is produced deep in the solar core and propagates adiabatically, it will follow the heavy mass trajectory, emerging from the sun as a ν_μ.

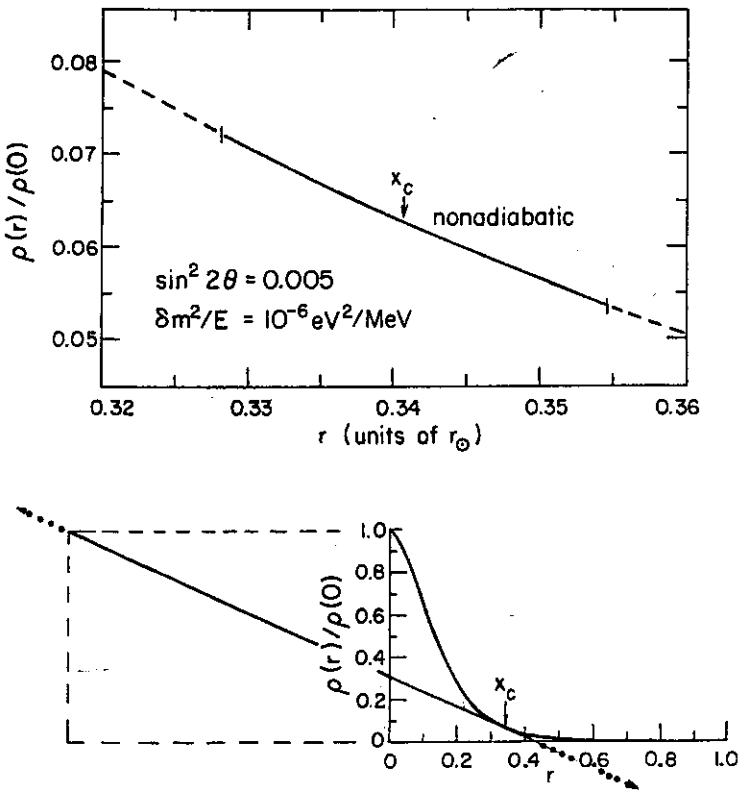

Figure 13 The top figure illustrates, for one choice of $\sin^2\theta_v$ and δm^2, that the region of nonadiabatic propagation (*solid line*) is usually confined to a narrow region about the crossing point x_c. In the lower figure, the solid lines represent the solar density $\rho(x)$ and a linear approximation to $\rho(x)$ that has the correct initial and final densities and the correct slope at x_c. (Thus the linear and exact density would almost exactly correspond over the nonadiabatic region illustrated in the upper figure). The MSW equation can be solved analytically for the linear wedge. By extending the wedge to $\pm\infty$ (*dotted lines*) and assuming adiabatic propagation in those regions of unphysical density, one obtains the simple Landau-Zener result of Equations (31) and (32).

functions, respectively. This treatment, called the finite Landau-Zener approximation (Haxton 1987, Petcov 1988) has been used extensively in numerical calculations.

We derive a simpler ("infinite") Landau-Zener approximation (Landau 1932, Zener 1932) by observing that the nonadiabatic region is generally confined to a narrow region around x_c, away from the endpoints x_i and x_f. We can then extend the artificial profile to $x = \pm\infty$, as illustrated by the dashed lines in Figure 13. This permits one to replace the parabolic cylinder or Whittaker functions of the finite Landau-Zener approximation by their much simpler asymptotic forms.

As the neutrino propagates adiabatically in the unphysical region $x < x_i$, the exact solution in the physical region can be recovered by choosing the initial boundary conditions

$$a_L(-\infty) = -a_\mu(-\infty) = \cos\theta_i \exp\left[-i\int_{-\infty}^{x_i}\lambda(x)dx\right],$$

$$a_H(-\infty) = a_e(-\infty) = \sin\theta_i \exp\left[i\int_{-\infty}^{x_i}\lambda(x)dx\right]. \quad (30)$$

That is, $|\nu(-\infty)\rangle$ will then adiabatically evolve to $|\nu(x_i)\rangle = |\nu_e\rangle$ as x goes from $-\infty$ to x_i. The unphysical region $x > x_f$ can be handled similarly.

With some algebra a simple generalization of the adiabatic result emerges that is valid for all $\delta m^2/E$ and θ_v:

$$P_{\nu_e} = \frac{1}{2} + \frac{1}{2}\cos 2\theta_v \cos 2\theta_i (1 - 2P_{hop}), \quad (31)$$

where P_{hop} is the probability of hopping from the heavy mass trajectory to the light trajectory on traversing the crossing point. For the linear approximation to the density,

$$P_{hop}^{lin} = e^{-\pi\gamma_c/2}. \quad (32)$$

As it must by our construction, P_{ν_e} reduces to $P_{\nu_e}^{adiab}$ for $\gamma_c \gg 1$. P_{hop}^{lin} was derived by Haxton (1986) and independently by Parke (1986), who married this approximation to the adiabatic one to get Equation (31). The exponential hopping probability, first obtained by Petcov (1988), is

$$P_{hop}^{exp} = \frac{e^{-\pi\delta(1-\cos 2\theta_v)} - e^{-2\pi\delta}}{1 - e^{-2\pi\delta}}, \quad (33)$$

where $\delta = (\gamma_c \cos 2\theta_v)/(\sin^2 2\theta_v)$. Note that for small θ_v, $\delta(1 - \cos 2\theta_v) \to \gamma_c/2$ and $\delta \to \gamma_c/(2\theta_v)^2$, so that Equations (32) and (33) then coincide. When the crossing becomes nonadiabatic [e.g. $\gamma_c \ll 1$ in Equation (32)], the hopping probability goes to 1, allowing the neutrino to exit the sun on the light mass trajectory as a ν_e, i.e. no conversion occurs.

Thus there are two conditions for strong conversion of solar neutrinos: there must be a level crossing [that is, the solar core density must be sufficient to render $\nu_e \sim \nu_H(x_i)$ when it is first produced] and the crossing must be adiabatic. The first condition requires that $\delta m^2/E$ not be too large, and the second that $\gamma_c \gtrsim 1$. The combination of these two constraints, illustrated in Figure 14, defines a triangle of interesting parameters in the $(\delta m^2)/E - \sin^2 2\theta_v$ plane, as Mikheyev & Smirnov and others (Rosen & Gelb 1986) found by numerically integrating Equation (20). A remarkable feature of this triangle is that strong $\nu_e \to \nu_\mu$ conversion can occur for very small mixing angles ($\sin^2 2\theta \sim 10^{-3}$), unlike the vacuum case.

One can envision superimposing on Figure 14 the spectrum of solar neutrinos, plotted as a function of $(\delta m^2)/E$ for some choice of δm^2. Because Davis sees *some* solar neutrinos, the solutions must correspond to the boundaries of the triangle in Figure 14. The horizontal boundary indicates the maximum $(\delta m^2)/E$ for which the sun's central density is sufficient to cause a level crossing. If a spectrum properly straddles this boundary, we obtain a result consistent with the Homestake experiment in which low-energy neutrinos (large $1/E$) lie above the level-crossing boundary (and thus remain ν_e s), but the high-energy neutrinos (small $1/E$) fall within the unshaded region where strong conversion takes place. Such a solution thus mimics nonstandard solar models in that only the ^{8}B neutrino flux would be strongly suppressed. The diagonal boundary separates the adiabatic and nonadiabatic regions. If the spectrum straddles

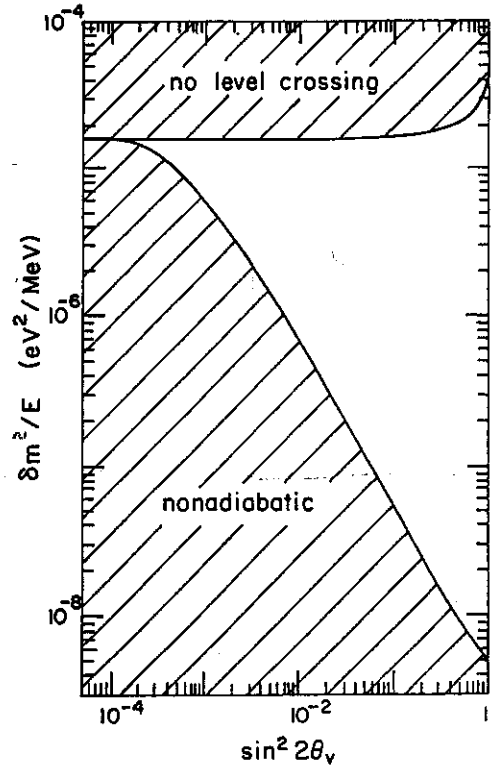

Figure 14 MSW conversion for a neutrino produced at the sun's center. The upper shaded region indicates those $\delta m^2/E$ where the vacuum mass splitting is too great to be overcome by the solar density. Thus, no level crossing occurs. The lower shaded region defines the $(\delta m^2)/E - \sin^2 2\theta_v$ region where the level crossing is nonadiabatic ($\gamma_c < 1$). The unshaded region corresponds to adiabatic level crossings and thus to strong $\nu_e \to \nu_\mu$ conversion.

this boundary, we obtain a second solution in which low-energy neutrinos lie within the conversion region, but the high-energy neutrinos (small $1/E$) lie below the conversion region and are characterized by $\gamma \ll 1$ at the crossing density. [Of course, the boundary is not a sharp one, but is characterized by the exponential of Equation (32).] Such a nonadiabatic solution is quite distinctive because the flux of pp neutrinos, which is strongly constrained in the standard solar model and in any steady-state nonstandard model by the solar luminosity, would now be sharply reduced. Finally, one can imagine hybrid solutions in which the spectrum straddles both the level-crossing (horizontal) boundary and the adiabaticity (diagonal) boundary for small θ, thereby reducing the ^{7}Be neutrino flux more than either the pp or ^{8}B fluxes.

What are the results of a careful search for MSW solutions satisfying the Homestake, Kamiokande, and SAGE/GALLEX constraints? Figure 15 is a calculation by Hata (1995) (also see Hata & Langacker 1994) for flavor oscillations that includes the effects of terrestrial regeneration. (MSW effects can occur as the neutrinos pass through the Earth.) The preferred (in the sense of minimizing the χ^2) solution, corresponding to a region surrounding $\delta m^2 \sim 6 \cdot 10^{-6}$ eV^2 and $\sin^2 2\theta_v \sim 6 \cdot 10^{-3}$, is the hybrid case described above. It is commonly referred to as the small-angle solution. A second, large-angle solution exists, corresponding to $\delta m^2 \sim 10^{-5}$ eV^2 and $\sin^2 2\theta_v \sim 0.6$, but this region of Figure 15 has shrunk as the precision of the gallium experiments improve.

These solutions can be distinguished by their characteristic distortions of the solar neutrino spectrum. The survival probabilities $P_{\nu_e}^{\rm MSW}(E)$ for the small- and large-angle parameters given above are shown as a function of E in Figure 16.

The calculations of Figure 14 assume flavor oscillations into a ν_μ or ν_τ. This influences the interpretation of the Kamiokande experiment, as heavy flavor neutrinos contribute to elastic scattering. Another possibility is an oscillation into a sterile neutrino. The large-angle solution is then ruled out by the Kamiokande requirement of a large ν_e survival probability (see, for example, Hata 1995, Barger et al 1991). It is also ruled by the neutrino counting limit from big bang nucleosynthesis (Barbieri & Dolgov 1991; Enqvist el al 1990; Shi, Schramm & Fields 1993).

The MSW mechanism provides a natural explanation for the pattern of observed solar neutrino fluxes. Although it requires profound new physics, both massive neutrinos and neutrino mixing are expected in extended models. The preferred solutions correspond to $\delta m^2 \sim 10^{-5}$ eV^2 and thus are consistent with $m_2 \sim$ few 10^{-3} eV. This is a typical ν_τ mass in models where $m_{\rm R} \sim m_{\rm GUT}$. On the other hand, if it is the ν_μ participating in the oscillation, this gives $m_{\rm R} \sim 10^{12}$ GeV and predicts a heavy $\nu_\tau \sim 10$ eV (Bludman, Kennedy & Langacker 1992). Such a mass is of great interest cosmologically as it would have consequences for supernova neutrinos (Fuller et al 1992, Qian et al 1993), the dark matter problem, and the formation of large-scale structure.

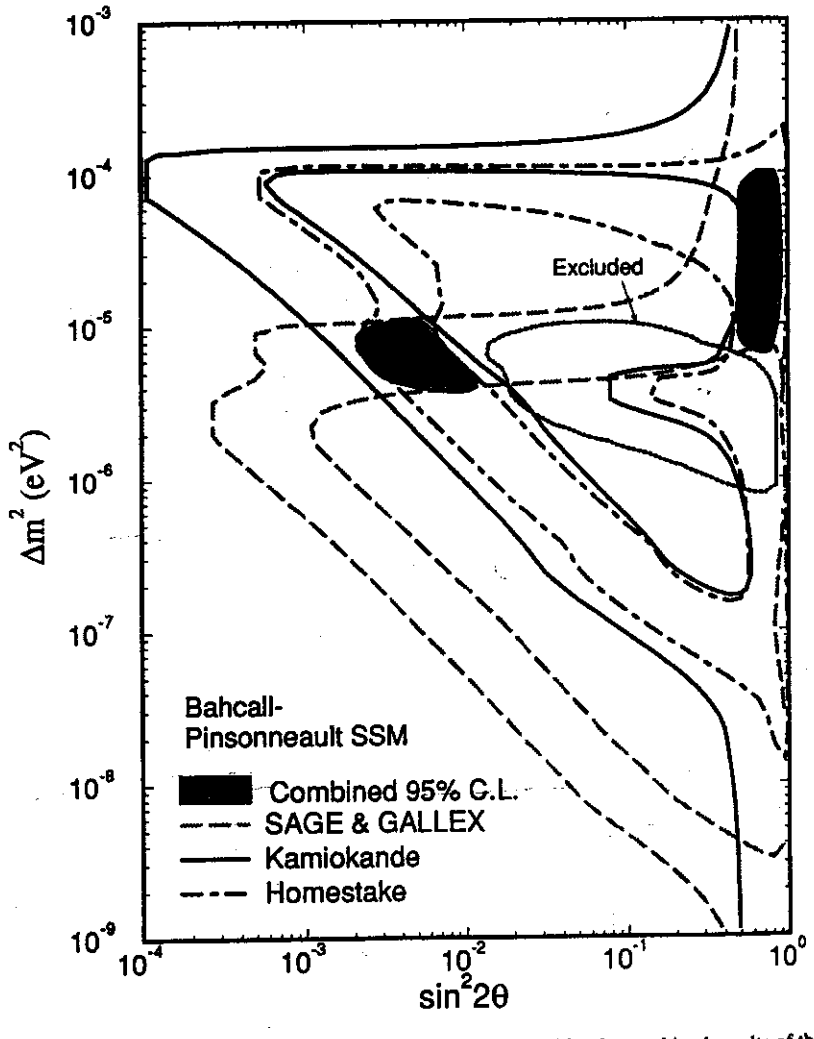

Figure 15 The MSW solutions allowed at 95% confidence level by the combined results of the Homestake, SAGE/GALLEX, and Kamiokande experiments, including Kamiokande II day-night constraints, given the BP flux predictions. (From Hata 1995.)

If the MSW mechanism proves not to be the solution of the solar neutrino problem, it still will have greatly enhanced the importance of solar neutrino physics: The existing experiments have ruled out large regions in the $\delta m^2 - \sin^2 2\theta_v$ plane (corresponding to nearly complete $\nu_e \rightarrow \nu_\mu$ conversion) that remain hopelessly beyond the reach of accelerator neutrino oscillation experiments.

4.3 *Other Particle Physics Scenarios*

Several other intriguing particle physics phenomena could affect the solar neutrino puzzle. The upper bound established in the earliest ^{37}Cl runs was consistent with the complete absence of solar neutrinos, prompting the suggestion that the ν_e might decay before reaching Earth (Bahcall, Cabibbo & Yahil 1972). This requires a nonzero neutrino mass and a sufficiently fast decay mode. The suggestion is less appealing given the present pattern of fluxes: If the lifetime is arranged to allow some neutrinos to survive, one expects the low-energy neutrino flux to be more severely suppressed than that of the high-energy neutrinos. There is also the constraint from supernova SN1987A, where $\bar{\nu}_e$s successfully traveled 50 kpc. However, one can still wiggle out of both objections if the neutrino decay is catalyzed by matter effects

$$\nu_e \underset{\text{MSW}}{\rightarrow} \nu_2 \rightarrow \text{decay products} \tag{34}$$

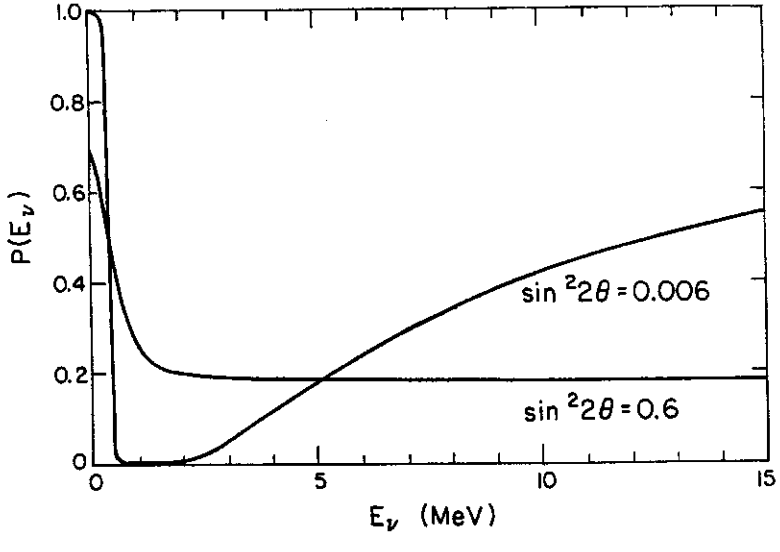

Figure 16 MSW survival probabilities $P^{\text{MSW}}_{\nu_e}(E)$ for typical small-angle ($\delta m^2 \sim 6 \cdot 10^{-6}$ eV^2, $\sin^2 2\theta_v \sim 6 \cdot 10^{-3}$) and large-angle ($\delta m^2 \sim 10^{-5}$ eV^2, $\sin^2 2\theta_v \sim 0.6$) solutions.

as Raghavan, He & Pakvasa suggested (1988). The spectrum distortions do not necessarily mimic the MSW mechanism because the decay probability can depend on the neutrino energy.

Weakly interacting massive particles (WIMPs) were suggested (Faulkner & Gilliland 1985, Spergel & Press 1985) as a simultaneous solution to the solar neutrino and dark matter problems. If a heavy neutral particle has a mean free path (at solar densities) comparable to the solar diameter, it can lose energy in transit and be captured in the sun's gravitational field. Once the sun accumulates a sufficiently dense cloud of such particles, they contribute to energy transport in the sun, thus violating the SSM assumption that only radiative transport is important in the core. The WIMP can pick up energy by scattering off faster core nucleons, then lose it by rescattering in the cooler outer layers of the sun. The additional transport lowers the core temperature. While this suggestion is clever, a simple lowering of T_c is no longer sufficient to reconcile the SSM with experiment.

Perhaps the most interesting possibility, apart from the MSW mechanism, was stimulated by suggestions that the ^{37}Cl signal might be varying with a period comparable to the 11-year solar cycle. While the evidence for this has weakened, the original claims generated renewed interest in neutrino magnetic moment interactions with the solar magnetic field.

The original suggestions by Cisneros (1971) and by Okun, Voloshyn & Vysotsky (1986) envisioned the rotation

$$\nu_{e_L} \rightarrow \nu_{e_R} \tag{35}$$

producing a right-handed neutrino with sterile interactions in the standard model. With the discovery of the MSW mechanism, it was realized that matter effects would break the vacuum degeneracy of the ν_{e_L} and ν_{e_R}, suppressing the spin precession. Lim & Marciano (1988) and Akhmedov (1988) pointed out that this difficulty was naturally circumvented for

$$\nu_{e_L} \rightarrow \nu_{\mu_R} \tag{36}$$

as the different matter interactions of the ν_e and ν_μ can compensate for the vacuum $\nu_e - \nu_\mu$ mass difference, producing a crossing similar to the usual MSW mechanism. Such spin-flavor precession can then occur at full strength due to an off-diagonal (in flavor) magnetic moment.

There has been a great deal of clever work on this problem (Minakata & Nunokawa 1989; Balantekin, Hatchell & Loreti 1990). A very strong limit on both diagonal and off-diagonal magnetic moments is imposed by studies of the red giant cooling process of plasmon decay into neutrinos,

$$\gamma^* \rightarrow \nu_i \bar{\nu}_j. \tag{37}$$

The result is $|\mu_{ij}| \lesssim 3 \cdot 10^{-12} \mu_B$, where μ_B is an electron Bohr magneton (Raffaelt 1990). With this bound, solar magnetic field strengths of $B_\odot \gtrsim 10^6$ G

are needed to produce interesting effects. Because the location of the Lim-Marciano level crossing depends on the neutrino energy, such fields have to be extensive to affect an appreciable fraction of the neutrino spectrum. It is unclear whether these conditions can occur in the sun.

There are interesting, related phenomena involving the effects of solar density fluctuations or currents on the MSW mechanism: One can drive $\nu_e \rightarrow \nu_\mu$ oscillations in the absence of a level crossing by harmonic density perturbations (not unlike adiabatic fast passage in nuclear magnetic resonance experiments) (Haxton & Zhang 1991, Schäfer and Koonin 1987, Krastev & Smirnov 1989). The effects of "white noise" density fluctuations on the MSW mechanism have also been examined recently (Loreti & Balantekin 1994). Such fluctuations generate a flavor analog of stochastic spin depolarization—a phenomenon familiar in atomic physics.

5. NEW EXPERIMENTS

The MSW mechanism has had a particularly strong impact because it was discovered at a time when new data (SAGE/GALLEX, Kamiokande, helioseismology) were eliminating many competing solutions to the solar neutrino problem. The physics of the MSW mechanism is both simple and elegant, which accounts for much of its appeal, but the most important attribute of this solution is that it can be definitively tested. The favored small-angle solution produces a distinctive distortion in the solar neutrino spectrum. Furthermore, if the oscillation is into another flavor (rather than into a sterile state), the missing neutrinos can be found through their neutral current interactions. These tests will be made by two high-statistic direct-counting directors now under construction.

5.1 *The Sudbury Neutrino Observatory (SNO)*

A water Cerenkov detector of a different type is under construction deep (5900 m.w.e.) within the Creighton #9 nickel mine at Sudbury, Ontario, Canada (Ewan et al 1987, Aardsma et al 1987, Chen 1985). The central portion of the detector is an acrylic vessel containing 1 kiloton of heavy water, D_2O. This is surrounded by 5 m of light water to protect the inner detector from neutrons and gammas. The detector is viewed by 9500 20-cm PMTs, which provide 56% photocathode coverage (Figure 17).

The D_2O introduces two new channels. The charged current breakup reaction

$$\nu_e + D \rightarrow p + p + e^- \tag{38}$$

produces a recoil electron that carries off almost all of the final-state kinetic energy. As the Gamow-Teller strength is concentrated very close to the p + p threshold, 1.44 MeV, the electron and neutrino energies are related by $E_\nu \sim E_e + 1.44$ MeV. Thus, neutrino spectrum distortions should show up

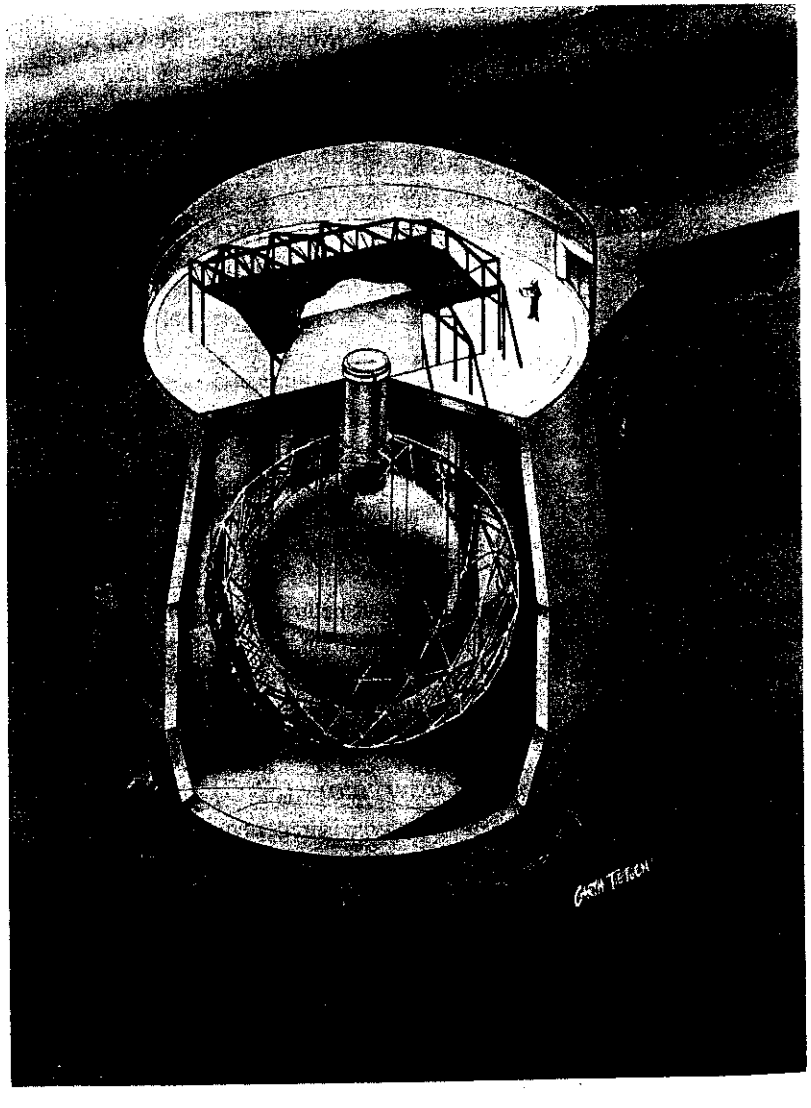

Figure 17 Schematic of the SNO detector now under construction in the Creighton #9 nickel mine, Sudbury. (Provided by RGH Robertson & JF Wilkerson; private communication.)

clearly in the measured electron energy distribution. As the GT strength in the deuteron is equivalent to about one third of that of a free neutron, the anticipated counting rates are high. For an electron detection threshold of 5 MeV and a ^{8}B neutrino flux equal to 51% of the BP SSM value, 3300 events will be recorded each year.

A second channel is equally sensitive to neutrinos of any flavor,

$$\nu_x + \mathrm{D} \rightarrow \nu_x' + \mathrm{n} + \mathrm{p}, \tag{39}$$

and thus will be crucial in testing whether flavor oscillations have occurred. The anticipated event rate is approximately 2000/year in the BP SSM. The addition of $MgCl_2$ to the D_2O at a concentration of 0.2–0.3% allows the neutrons to be observed by ^{35}Cl(n,γ). The Cerenkov light produced by the showering of the 8.6 MeV capture γ ray will add to the signal from the charged current reaction. By operating the detector with and without salt, the experimenters will separate the charged and neutral current signals. The SNO collaboration also plans to deploy proportional counters filled with ^{3}He to exploit the neutron-specific charge-exchange reaction ^{3}He(n,p)^{3}H. With such detectors, SNO will be sensitive to neutral current events at all times.

The detection of ~8 neutrons/day in a kiloton detector places extraordinary constraints on radiopurity. For example, a potentially serious background source is the photodisintegration of deuterium by energetic photons from U and Th chains. The experimental goal is concentrations of $\lesssim 10^{-14}$ grams of U and Th per gram of D_2O.

SNO is scheduled to begin operations in mid-1996.

5.2 *Superkamiokande*

Superkamiokande will be a greatly enlarged version of Kamiokande II/III with improved threshold (5 MeV) and energy and position resolution (Totsuka 1987, 1990; Takita 1993). It is currently under construction in the Kamioka mine at a depth of 2700 m.w.e. (see Figure 18).

The fiducial volume for detecting solar neutrinos will be 22 kilotons; this compares to 0.68 kilotons in the existing detector. This enlargement plus the improved threshold will increase the detection rate for neutrino-electron scattering by a factor of ~90, to 8400/year. Despite the soft kinematics of the ν_e-e reaction, the experimenters believe the high statistics will allow them to distinguish the spectral distortions produced by competing MSW solutions.

Because elastic scattering is sensitive to both ν_e and heavy-flavor neutrinos (in the ratio of 7:1), an accurate SNO determination of the ν_e spectrum will allow Superkamiokande to extract the spectrum of ν_μs or ν_τs.

Superkamiokande construction is scheduled to be completed in March 1996.

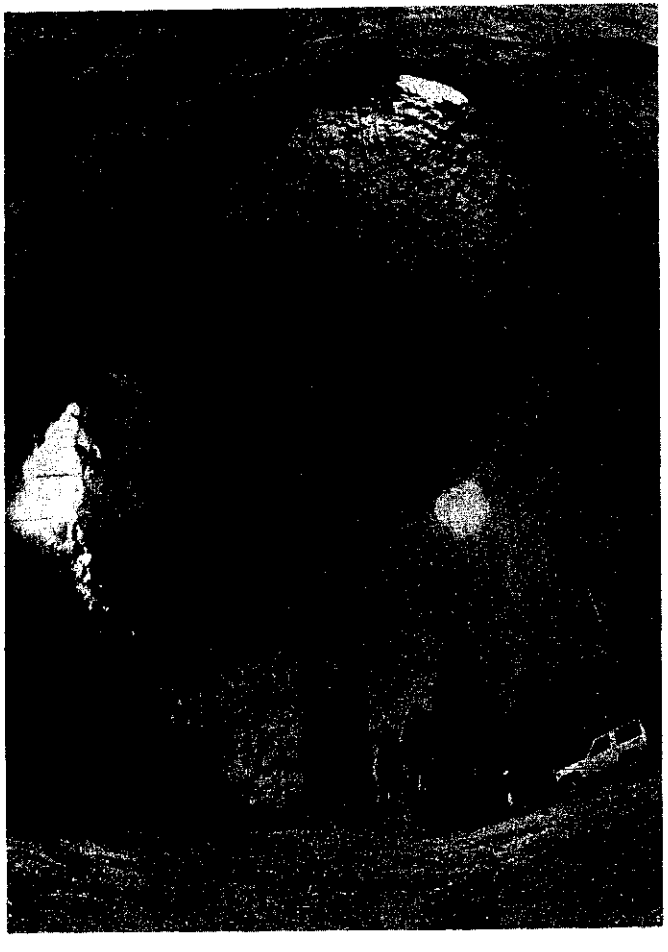

Figure 18 Photograph of the Kamioka Mine cavity that will house Superkamiokande. (Photo provided by the Institute for Cosmic Ray Research, University of Tokyo.)

5.3 *Other Future Detectors*

The Borexino collaboration (Raghavan 1991, Campanella 1992) has proposed a 0.3-kiloton liquid scintillator for installation in the Gran Sasso Laboratory. The experimenters hope to detect ^{7}Be neutrinos by ν-e scattering. The detection of very low energy recoil electrons places stringent constraints on U, Th, K, and other activities in the detector, e.g. $\lesssim 10^{-16}$ g U/g, including a requirement for continuous purification. The experimenters will evaluate background problems in a test facility now under construction, which is scheduled to be completed by the end of 1995. The anticipated counting rate for the full-scale detector is $\sim$18,000 ^{7}Be neutrino events/year for the BP SSM.

A high-counting-rate twin of the ^{37}Cl detector utilizing the reaction ^{127}I(ν_e,e) ^{127}Xe has been funded recently and is under construction in the Homestake mine (Lande 1993, Haxton 1988b). With a threshold of 664 keV, the detector is primarily sensitive to ^{7}Be and ^{8}B neutrinos. The initial Homestake detector will contain 100 tons of iodine as a solution of NaI. A smaller version of this detector was recently used at the LAMPF beamstop to measure the ^{127}I cross section for stopped muon decay ν_es. Calibration of the ^{7}Be neutrino cross section by an ^{37}Ar neutrino source is also planned. The 100-ton detector is scheduled to be completed by the end of 1995, with plans for an expansion to 1 kiloton afterwards.

A 5-kiloton liquid argon time-projection chamber, ICARUS II, has been proposed for Gran Sasso (Rubia 1985). In addition to ν-e scattering, the charged current channel

$$\nu_e + {}^{40}\mathrm{Ar} \rightarrow e^- + {}^{40}\mathrm{K}^* \hookrightarrow {}^{40}\mathrm{K} + \gamma \tag{40}$$

will allow the experimenters to measure the shape of the high-energy portion of the ^{8}B ν_e spectrum.

There are a number of important development efforts underway that focus on new technologies for the next generation of solar neutrino detectors; the reader is referred to the recent review by Lanou (1995). There are significant challenges motivating these efforts, e.g. neutrino detection by coherent scattering off nuclei and real-time detectors for pp neutrinos, such as the superfluid ^{4}He detector HERON (Bandler et al 1992) and the high-pressure helium time-projection chamber HELLAZ (Bonvicini 1994, Laurenti et al 1994).

6. OUTLOOK

The successes of the Kamiokande and SAGE/GALLEX experiments have led to a more complicated solar neutrino problem. The apparent strong suppression of the ^{7}Be flux (negative in most unconstrained fits!) is not a result expected by those who favored nonstandard solar model solutions to the ^{37}Cl puzzle.

Perhaps this is telling us that solar modelers have not been sufficiently inventive in modifying the SSM, but it may also be a push to look elsewhere for the solution.

We do have one candidate solution that works extremely well: the MSW mechanism. The required new physics has deep implications for particle physics and cosmology. Yet this physics is not exotic—the requirements of massive neutrinos and mixing are common assumptions in extensions of the standard electroweak model. The elegance of this solution makes it difficult to maintain one's scientific skepticism: The notion that the sun was perfectly designed to enhance the mixing of neutrinos with GUT-scale seesaw masses has too great an emotional appeal.

Fortunately, the solution to the solar neutrino problem does not have to be decided by community vote; the issue will be resolved by hard-nosed experimentation. SNO and Superkamiokande are just a year away, and they may crack this 30-year-old problem. Yet these are difficult experiments, and the physics they address is fundamental to two of our standard models (particle and solar). It is prudent for the community to continue to seek cross-checks on these and other future measurements. As has proven true in the past, there is no guarantee that the SNO and Superkamiokande results will conform to our expectations.

ACKNOWLEDGMENTS

I am indebted to the participants of the Seattle Solar Modeling Workshop for much of the background material that was incorporated into this paper. It is a special pleasure to thank J Bahcall, AB Balantekin, B Cleveland, R Davis Jr, S Degl'Innocenti, N Hata, C Johnson, K Lande, K Nakamura, S Parke, P Parker, Y-Z Qian, H Robertson, Y Totsuka, and J Wilkerson for helpful discussions and assistance. This work was supported in part by the US Department of Energy and by NASA under grant #NAGW2523.

Literature Cited

Aardsma G, Allan RC, Anglin JD, Bercovitch M, Carter AL, et al. 1987. *Phys. Lett. B* 194:321–25
Abdurashitov JN, Faizov EL, Gavrin VN, Gusev AO, Kalikov AV, et al. 1994. *Phys. Lett. B* 328:234–48
Abraham Z, Iben I Jr. 1971. *Ap. J.* 170:157–63
Adelberger EG, Haxton WC. 1987. *Phys. Rev. C* 36:879–82
Akhmedov EKh. 1988. *Sov. J. Nucl. Phys.* 48:382–83; *Phys. Lett.* 213:64–68
Alvarez LW. 1949. *Univ. Calif. Rad. Lab. Rep. UCRL-328* (Unpubl.)
Alvarez LW. 1973. *Lawrence Rad. Lab. Phys. Notes* Memo #767
Anselmann P, Frockenbrock R, Hampel W, Heusser G, Kiko J, et al. 1995. *Phys. Lett. B* In press

Anselmann P, Hampel W, Heusser G, Kiko J, Kirsten T, et al. 1992. *Phys. Lett. B* 285:376–89
Anselmann P, Hampel W, Heusser G, Kiko J, Kirsten T, et al. 1994. *Phys. Lett. B* 327:377–85
Assenbaum HJ, Langanke K, Rolfs C. 1987. *Z. Phys. A* 327:461–68
Austin SM, Anantaraman N, Love WG. 1994. *Phys. Rev. Lett.* 73:30–33
Babu KS, Mohapatra RN. 1993. *Phys. Rev. Lett.* 70:2845–48
Bahcall JN. 1964a. *Phys. Rev. Lett.* 12:300–2
Bahcall JN. 1964b. *Phys. Rev. Lett.* 136:B1164–71
Bahcall JN. 1966. *Phys. Rev. Lett.* 17:398–401
Bahcall JN. 1989. *Neutrino Astrophysics.* Cambridge:Cambridge Univ. Press. 567 pp.
Bahcall JN. 1993. *Phys. Rev. Lett.* 71:2369–71
Bahcall JN. 1994. *Phys. Lett. B* 338:276–81
Bahcall JN, Bahcall NA, Shaviv G. 1968. *Phys. Rev. Lett.* 20:1209–12
Bahcall JN, Bethe H. 1990. *Phys. Rev. Lett.* 65:2233–35
Bahcall JN, Cabibbo N, Yahil A. 1972. *Phys. Rev. Lett.* 28:316–18
Bahcall JN, Davis R Jr. 1982. In *Essays in Nuclear Astrophysics,* ed. CA Barnes, DD Clayton, D Schramm, p. 243. Cambridge: Cambridge Univ. Press. 562 pp.
Bahcall JN, Haxton WC. 1989. *Phys. Rev. D* 40:931–41
Bahcall JN, Holstein BR. 1986. *Phys. Rev. C* 33:2121–27
Bahcall JN, Pinsonneault MH. 1992. *Rev. Mod. Phys.* 64:885–926 (BP)
Bahcall JN, Pinsonneault MH. 1995. *Rev. Mod. Phys.* Submitted
Bahcall JN, Ulrich RK. 1971. *Ap. J.* 170:593–603
Bahcall JN, Ulrich RK. 1988. *Rev. Mod. Phys.* 60:297–372 (BU)
Balantekin AB, Bahcall JN, eds. 1995. *Proc. Solar Modeling Workshop.* Singapore: World Scientific. In press
Balantekin AB, Hatchell PJ, Loreti F. 1990. *Phys. Rev. D* 41:3588–93
Bandler SR, Lanou RE, Maris HJ, More T, Porter FS, et al. 1992. *Phys. Rev. Lett.* 68:2429–32
Barbieri R, Dolgov A. 1991. *Nucl. Phys. B* 349:743–53
Barger V, Deshpande N, Pal PB, Phillips RJN, Whisnant K. 1991. *Phys. Rev. D* 43:1759–62
Barker FC. 1980. *Aust. J. Phys.* 33:177–90
Bartenwerfer D. 1973. *Astron. Astrophys.* 25:455–56
Bethe H. 1986. *Phys. Rev. Lett.* 56:1305–8
Bludman SA, Kennedy DC, Langacker PG. 1992. *Phys. Rev. D* 45:1810–13
Bonvicini G. 1994. *Nucl. Phys. B* 35:438 (Proc. Suppl.)
Bowles TJ, Gavrin VN. 1993. *Annu. Rev. Nucl. Part. Sci.* 43:117–64
Burbidge EM, Burbidge GR, Fowler WA, Hoyle F. 1957. *Rev. Mod. Phys.* 29:547
Campanella M. 1992. In *Proc. 3rd Int. Workshop on Neutrino Telescopes,* ed. M Baldo-Ceolin, p. 73. Venice: Univ. Padova
Castellani V, Degl'Innocenti S, Fiorentini G, Lissia M, Ricci B. 1994. JD, Bercovitch M,D 50:4749–61
Castellani V, Degl'Innocenti S, Fiorentini G, Ricci B. 1995. See Balantekin & Bahcall 1995
Charbonnel C. 1995. See Balantekin & Bahcall 1995
Chen HH. 1985. *Phys. Rev. Lett.* 55:534–36
Cherry ML, Fowler WA, Lande K, eds. 1985. JD, BeSolar Neutrinos and Neutrino Astronomy. New York: Am. Inst. Phys. 322 pp.
Christensen-Dalsgaard J, Gough DO. 1980. *Nature* 288:544–47
Christy RF, Duck I. 1961. *Nucl. Phys.* 24:89
Cisneros A. 1981. *Astrophys. Space Sci.* 10:87
Cowan GA, Haxton WC. 1982. *Science.* 216:51–54
Davis R Jr. 1985. See Cherry et al 1985, pp. 1–21
Davis R Jr. 1993. In *Frontiers of Neutrino Astrophysics,* ed. Y Suzuki, K Nakamura, p. 47. Tokyo: Univ. Acad. Press
Davis R Jr, Cleveland BT, Rowley JK. 1983. JIn *Science Underground,* ed. MM Nieto, WC Haxton, CM Hoffman, EW Kolb, VD Sandberg, JW Toevs, pp. 2–15. New York: Am. Inst. Phys. 446 pp.
Davis R Jr, Harmer DS, Hoffman KC. 1968. *Phys. Rev. Lett.* 20:1205–9
Demarque P, Mengel J, Sweigart A. 1973. *Ap. J.* 183:997–1004; JD, BeNature Phys. Sci. 246:33
Dilke FWW, Gough DO. 1972. *Nature* 240:262
Dimopoulos S, Hall LJ, Raby S. 1993. *Phys. Rev. D* 47:R3697–701
Enqvist K, Kainulainen K, Maalampi J. 1990. *Phys. Lett. B* 249:531–34
Ewan GT, Evans HC, Lee HW, Leslie JR, Mak HB, et al. 1987. *Queen's Univ. Rep. SNO-87-12*
Ezer D, Cameron AGW. 1968. *Astrophys. Lett.* 1:177–79
Faulkner J, Gilliland RL. 1985. *Ap. J.* 299:994–1000
Filippone BW, Elwyn AJ, Davids CN, Koetke DD. 1983. *Phys. Rev. Lett.* 50:412–6; *Phys. Rev. C* 28:2222–29
Fowler WA. 1972. *Nature* 238:24
Fowler WA. 1984. *Rev. Mod. Phys.* 56:149–79
Fuller GM, Mayle RW, Meyer BS, Wilson JR. 1992. *Ap. J.* 389:517–526
Gai M, Bertulani CA. 1994. Univ. Conn. Preprint 40870-0005
Garcia A, Adelberger EG, Mangus PV, Swanson HE, Tengblad HE, et al. 1991. *Phys. Rev. Lett.* 67:3654–57
Garcia A, Adelberger EG, Mangus PV, Swan-

son HE, Wells DP, et al. 1995. *Phys. Rev. C* 51:R439–42
Glashow SL, Krauss LM. 1987. *Phys. Lett. B* 190:199–207
Hampel W. 1985. See Cherry et al 1985, pp. 162–74
Hata N. 1995. See Balantekin & Bahcall 1995
Hata N, Haxton WC. 1995. *Phys. Lett. B* Submitted
Hata N, Langacker P. 1994. *Phys. Rev. D* 48:2937–40
Haxton WC. 1986. *Phys. Rev. Lett.* 57:1271–74
Haxton WC. 1987. *Phys. Rev. D* 35:2352–64
Haxton WC. 1988a. *Phys. Rev. C* 38:2474–77
Haxton WC. 1988b. *Phys. Rev. Lett.* 60:768–71
Haxton WC, Zhang W-M. 1991. *Phys. Rev. D* 43:2484–94
Hirata KS, Inoue K, Ishida T, Kajita T, Kihara K, et al. 1991. *Phys. Rev. D* 44:2241–60
Hirata KS, Kajita T, Koshiba M, Nakahata M, Oyama Y, et al. 1988. *Phys. Rev. D* 38:448–58
Iben I Jr. 1969. *Ann. Phys.* 54:164–203
Johnson CW, Kolbe E, Koonin SE, Langanke K. 1992. *Ap. J.* 392:320–27
Kavanagh RW, Tombrello TA, Mosher JM, Goosman DR. 1969. JD, BeBull. Am. Phys. Soc. 14:1209
Kavanagh RW. 1972. In *Cosmology, Fusion, and Other Matters*, ed. F Reines. Boulder: Colo. Assoc. Univ. Press
Krastev PI, Smirnov A Yuit1989. *Phys. Lett. B* 226:341–46
Krauss A, Becker HW, Trautretter HP, Rolfs C. 1987. *Nucl. Phys. A* 467:273–90
Krofcheck D, Sugarbaker E, Rapaport J, Wang D, Bahcall JN, et al. 1985. *Phys. Rev. Lett.* 55:1051–54; JKrofcheck D. 1987. PhD thesis. Ohio State Univ.
Kuzmin VA. 1966. *Sov. Phys. JETP* 22:1051; JKuzmin VA, Zatsepin GT. 1966. *Proc. Int. Conf. on Cosmic Rays* 2:1023
Kwong W, Rosen SP. 1994. *Phys. Rev. Lett.* 73:369
Landau LD. 1932. *Phys. Z. Sowjetunion* 2:46
Lande K. 1993. *Proc. 22nd Int. Conf. on Cosmic Ray Physics*. In press
Lande K. 1995. In *Neutrino '94*, ed. A Dar, G Eilam, M GroneauitAmsterdam: North Holland
Langanke K. 1995. See Balantekin & Bahcall 1995
Langanke K, Shoppa TD. 1994. *Phys. Rev. C* 49:R1771–74
Lanou R. 1995. *Proc. Snowmass Workshop on Nuclear and Particle Astrophysics and Cosmology in the Next Millenium.* In press
Laurenti G, Tzamarias S, Bonvicini G, Krastev P, Zichichi A et al. 1994. INFN preprint
Lim CS, Marciano WJ. 1988. *Phys. Rev. D* 37:1368–73
Loreti FN, Balantekin AB. 1994. *Phys. Rev. D* 50:4762–70
Merryfield WJ. 1995. See Balantekin & Bahcall 1995
Merryfield WJ, Toomre J, Gough DO. 1990. *Ap. J.* 353:678–97; 1991. *Ap. J.* 367:658–65
Messiah A. 1986. In *Massive Neutrinos in Astrophysics and in Particle Physics*, ed. O Fackler, J Tran Thanh Van, pp. 373–89. Gif-sur-Yvette: Editions Frontières. 704 pp.
Michaud G. 1977. *Nature* 266:433–34
Mikheyev SP, Smirnov A Yuit1985. *Sov. J. Nucl. Phys.* 42:913–17
Mikheyev SP, Smirnov A Yuit1986. *Nuovo Cimento* 9C:17–26
Mikheyev SP, Smirnov A Yuit1989. *Prog. Part. Nucl. Phys.* 23:41–136
Minakata H, Nunokawa H. 1989. *Phys. Rev. Lett.* 63:121–24
Motobayashi T, Iwasa N, Ando Y, Kurokawa M, Murakami H, et al. 1994. *Phys. Rev. Lett.* 73:2680–83
Nakamura K. 1994. *Proc. Int. Conf. on Non-Accelerator Particle Physics* (India). In press
Nico JS. 1994. In *Neutrino '94*, ed. A Dar, G Eilam, M GroneauitAmsterdam: North Holland
Okun LB, Voloshin MB, Vysotsky MI. 1986. JD, BeSov. Phys. JETP 64:446–52; *Sov. J. Nucl. Phys.* 44:440–41
Opik EJ. 1953. *Contrib. Armagh Obs.* No. 9
Parke SJ. 1986. *Phys. Rev. Lett.* 57:1275–78
Parke SJ. 1995. *Phys. Rev. Lett.* 74:839–41
Parker EN. 1974. *Astrophys. Space Sci.* 31:261
Parker PD. 1968. *Ap. J.* 153:L85–86
Parker PD, Rolfs C. 1991. In *The Solar Interior and Atmosphere*, ed. A Cox, WC Livingston, MS Mathews, p. 31. Tucson: Univ. Ariz. Press
Petcov ST. 1988. *Phys. Lett. B* 200:373–79
Pontecorvo B. 1946. *Chalk River Rep. PD-205* (Unpubl.)
Pontecorvo B. 1958. *Sov. Phys. JETP* 7:172
Poskanzer AM, McPherson R, Esterlund RA, Reeder PL. 1966. *Phys. Rev.* 152:995–1001
Qian YZ, Fuller FM, Mayle R, Mathews GJ, Wilson JR, Woosley SE. 1993. *Phys. Rev. Lett.* 71:1965–68
Raffaelt G. 1990. *Phys. Rev. Lett.* 64:2856–58
Raghavan RS. 1991. In *Proc. 25th Int. Conf. High Energy Physics*, ed. KK Phua, Y Yamaguchi, p. 482. Japan: South Asia Theor. Phys. Assoc. & Phys. Soc.
Raghavan RS, He X-G, Pakvasa S. 1988. *Phys. Rev. D* 38:1317–20
Rhodes EL Jr, Ulrich RK, Simon GW. 1977. *Ap. J.* 218:901–19
Rosen SP, Gelb JM. 1986. *Phys. Rev. D* 34:969–79
Rubia C. 1985. *INFN Publ.* INFN/AE-85-7
Schäfer A, Koonin SE. 1987. *Phys. Lett. B* 185:417–20
Schatzman E, Maeder A. 1981. *Nature* 290:683–86
Sextro RA, Gough RA, Cerny J. 1974. *Nucl. Phys. A.* 234:130–56
Shaviv G, Salpeter EE. 1968. *Phys. Rev. Lett.* 21:1602–5
Shi X, Schramm D, Fields B. 1993. *Phys. Rev. D* 48:2563–72
Spergel DN, Press WH. 1985. *Ap. J.* 294:663–73
Suzuki Y. 1995. *Nucl. Phys. B.* 38:54–59 (Proc. Suppl.)
Takita M. 1993. In *Frontiers of Neutrino Astrophysics*, ed. Y Suzuki, K Nakamura, p. 135. Tokyo: Univ. Acad. Press
Totsuka Y. 1987. In *Proc. 7th Workshop on Grand Unification*, ed. J Arafune, p. 118. Singapore: World Scientific
Totsuka Y. 1990. In *Proc. Int. Symposium on Underground Physics Experiments*, ed. K Nakamura, p. 129. Tokyo: Univ. Tokyo
Turck-Chièze S, Cahen S, Cassé M, Doom C. 1988. *Ap. J.* 335:415–24
Turck-Chièze S, Lopez I. 1993. *Ap. J.* 408:347–67 (TCL)
Ulrich RK. 1974. *Ap. J.* 188:369–78
Vaughn FJ, Chalmers RA, Kohler D, Chase LF. 1970. *Phys. Rev. C* 2:1057–65
Walker TP, Steigman G, Schramm DN, Olive KA, Kang H-S. 1991. *Ap. J.* 376:51–69
White M, Krauss L, Gates E. 1993. *Phys. Rev. Lett.* 70:375–78
Williams RD, Koonin SE. 1981. *Phys. Rev. C* 23:2773–74
Wolfenstein L. 1978. *Phys. Rev. D* 17:2369–74; 1979. JD, Bercovitch M,D 20:2634–35
Wolfsberg K, Cowan GA, Bryant EA, Daniels KS, Downey SW, et al. 1985. See Cherry et al 1985, pp. 196–202
Xu HM, Gagliardi CA, Tribble RE, Mukhamedzhanov AM, Timofeyuk NK. 1994. *Phys. Rev. Lett.* 73:2027–30
Zener C. 1932. *Proc. R. Soc. London Ser. A* 137:696